Published in final edited form as:
Neuroimage. 2007 September 1; 37(3): 731. doi:10.1016/j.neuroimage.2007.06.002.

A Novel Integrated MEG and EEG Analysis Method for Dipolar Sources

Ming-Xiong Huang[a,b,c,*], **Tao Song**[a], **Donald J. Hagler Jr.**[a], **Igor Podgorny**[d], **Veikko Jousmaki**[e], **Li Cui**[a], **Kathleen Gaa**[a], **Deborah L. Harrington**[a,c], **Anders M. Dale**[a,d], **Roland R. Lee**[a,b], **Jeff Elman**[f], and **Eric Halgren**[a,d]

[a] Department of Radiology, University of California, San Diego, San Diego, CA, USA [b] Radiology Service, VA San Diego Healthcare System, San Diego, CA, USA [c] Research Service, VA San Diego Healthcare System, San Diego, CA, USA [d] Department of Neuroscience, University of California, San Diego, San Diego, CA, USA [e] Brain Research Unit, Low Temperature Laboratory, Helsinki University of Technology, Otakaari 3 A, P.O. Box 2200, FIN-02015 HUT, Finland [f] Department of Cognitive Science, University of California, San Diego, San Diego, CA, USA

Abstract

The ability of magnetoencephalography (MEG) to accurately localize neuronal currents and obtain tangential components of the source is largely due to MEG's insensitivity to the conductivity profile of the head tissues. However, MEG cannot reliably detect the radial component of the neuronal current. In contrast, the localization accuracy of electroencephalography (EEG) is not as good as MEG, but EEG can detect both the tangential and radial components of the source. In the present study, we investigated the conductivity dependence in a new approach that combines MEG and EEG to accurately obtain, not only the location and tangential components, but also the radial component of the source. In this approach, the source location and tangential components are obtained from MEG alone, and optimal conductivity values of the EEG model are estimated by best-fitting EEG signal, while precisely matching the tangential components of the source in EEG and MEG. Then, the radial components are obtained from EEG using the previously estimated optimal conductivity values. Computer simulations testing this integrated approach demonstrated two main findings. First, there are well-organized optimal combinations of the conductivity values that provide an accurate fit to the combined MEG and EEG data. Second, the radial component, in addition to the location and tangential components, can be obtained with high accuracy without needing to know the precise conductivity profile of the head. We then demonstrated that this new approach performed reliably in an analysis of the 20-ms component from human somatosensory responses elicited by electric median-nerve stimulation.

Keywords

MEG; EEG; integration; conductivity; skull; tangential; radial; median nerve stimulation; somatosensory evoked field; somatosensory evoked potential; inverse problem

*Correspondence: Ming-Xiong Huang, Ph.D., Radiology Imaging Laboratory, Department of Radiology, University of California, San Diego, 3510 Dunhill Street, San Diego, CA 92121, Tel: 858-534-1254, Fax: 858-552-7404, mxhuang@ucsd.edu.

Introduction

MEG and EEG are functional imaging techniques that directly detect neuronal activity with millisecond temporal resolution. Previous studies have shown that integrating MEG and EEG is more beneficial than using each modality alone (Cohen and Cuffin, 1983; Cohen and Cuffin, 1987; Baillet et al., 1999; Huizenga et al., 2001; Goncalves et al., 2003a; Babiloni et al., 2004). Many studies indicate that MEG's ability to accurately locate neuronal sources is primarily due to its insensitivity to the conductivity profile of the head tissues. MEG localization accuracy is typically about 3mm in spherical phantom studies (Barth et al., 1986; Janday and Swithenby, 1987; Hansen et al., 1988; Yamamoto et al., 1988). While early studies using skull phantoms suggested that MEG localization accuracy was in the range of 4–8 mm (Barth et al., 1986; Weinberg et al., 1986; Janday and Swithenby, 1987; Yamamoto et al., 1988), a more rigorously designed human skull phantom study using 32 dipoles reported that MEG localization accuracy was about 3 mm (Leahy et al., 1998), similar to spherical phantoms. In contrast, EEG localization accuracy is about 8–10 mm using phantoms (Henderson et al., 1975; Leahy et al., 1998) and 10–20 mm using implanted electrodes in epilepsy patients (Smith et al., 1983; Smith et al., 1985; Cuffin et al., 1991; Cuffin, 1996; Krings et al., 1999). In all these studies, the number of MEG sensors and/or EEG electrodes was sufficiently larger than that of the dipole parameters. In empirical studies, EEG's localization accuracy is mainly affected by the errors of the estimated conductivity profile of the head. If the conductivity profile were precisely known, the EEG localization accuracy could be at least as good as that of the MEG (Liu et al., 2002).

MEG can also accurately obtain the tangential components of the neuronal current (Cohen and Cuffin, 1983; Cohen and Cuffin, 1987; Leahy et al., 1998; Huizenga et al., 2001; Goncalves et al., 2003a), but cannot reliably obtain the radial component of neuronal current that is perpendicular to the inner skull surface. In contrast, EEG is sensitive to both the tangential and radial components of the neuronal current. However, as noted above, accurate estimation of these components with EEG depends on precise knowledge of the source location and conductivity profile of the head tissues, particularly the skull (Pohlmeier et al., 1997; van den Broek et al., 1998; Ollikainen et al., 1999).

Usually, a piece-wise homogeneous approximation is adopted in EEG head models (based on a spherical model or more realistic Boundary Element Method (BEM) model), in which effective conductivities of the scalp, skull, and brain must be estimated (Mosher et al., 1999). The conductivities of the scalp and brain cannot be determined independently from extracranial measures (an ill-posed problem) and hence, they are usually assumed to be the same in most investigations (Nicholson, 1965; Geddes and Baker, 1967; Kosterich et al., 1983; Oostendorp et al., 2000; Goncalves et al., 2003a; Goncalves et al., 2003b; Lai et al., 2005), and the conductivity of the skull is assigned to be much lower than those of the scalp and the brain. In the case of MEG, a single layer that models the inner skull surface is quite accurate without knowledge of the conductivity profile of the skull and scalp (Hamalainen and Sarvas, 1989).

There are several approaches to analyzing simultaneous recordings from MEG and EEG (Brenner et al., 1978; Cohen and Cuffin, 1983; Cohen and Cuffin, 1987; Baillet et al., 1999; Huizenga et al., 2001; Goncalves et al., 2003a; Babiloni et al., 2004). In studies of somatosensory responses (Brenner et al., 1978; Cohen and Cuffin, 1983), the dipole locations in a spherical head model were separately obtained from MEG and EEG, and MEG showed better localization than EEG. Tangential dipole components can be obtained from MEG reliably whereas the radial component can be obtained from EEG with one set of pre-assigned conductivity values (Cohen and Cuffin, 1983). Several studies have also investigated different approaches of integrating MEG and EEG. Babiloni and colleagues (Babiloni et al., 2004) have shown that with a variable signal-to-noise ratio, the combined MEG and EEG analysis

performed better than each modality alone (Babiloni et al., 2004). The integrated MEG and EEG analysis suggested by Huizenga and colleagues (Huizenga et al., 2001) used a noise covariance matrix and estimated conductivities. The main concern, though, has been that the less-accurate EEG localization and unreliable MEG radial moment may systematically spoil the performance of the other imaging modality without any consequent improvement. Baillet and colleagues (Baillet et al., 1999) suggested a method for a cooperative processing of MEG and EEG in a distributed source model, which minimizes the mutual information between these two modalities. Goncalves and colleagues (Goncalves et al., 2003a), on the other hand, treated the dipole location and tangential dipole moments obtained from MEG as known parameters when fitting the EEG data by adjusting the conductivities of the brain (σ_{brain}), scalp (σ_{scalp}), and skull (σ_{skull}).

The major challenge remaining for combining MEG and EEG is the large variation in the estimated σ_{brain}, σ_{scalp}, and particularly σ_{skull}. Published values for σ_{brain} range from 0.12 to 0.48 S/m (Nicholson, 1965; Goncalves et al., 2003a; Goncalves et al., 2003b), and σ_{skull} range from 0.006 to 0.015 S/m (Geddes and Baker, 1967; Kosterich et al., 1983; Oostendorp et al., 2000; Goncalves et al., 2003a; Goncalves et al., 2003b). It is generally accepted that the $\sigma_{brain}/\sigma_{skull}$ ratio is the key factor in EEG source analysis (for a review see (Lai et al., 2005)). However, the impact of less-accurate estimations of the conductivity profile for an integrated MEG and EEG analysis is largely unclear. For example, in two integrated MEG and EEG studies from median-nerve responses in human, the $\sigma_{brain}/\sigma_{skull}$ ratio in one study was about 80 (Cohen and Cuffin, 1983); whereas in another study the ratio fell considerably, ranging between 43 to 86 in five human cases (average 72, SD = 48%) (Goncalves et al., 2003a). This finding raises three questions that have not been addressed systematically: 1) Why there is a wide range of $\sigma_{brain}/\sigma_{skull}$ ratios across subjects and studies that all appear to fit integrated MEG and EEG data equally well? 2) With such a discrepancy in the $\sigma_{brain}/\sigma_{skull}$ ratios in the literature, is it still possible to accurately obtain the source moments in an integrated MEG and EEG analysis? 3) Does the outcome of an integrated MEG and EEG analysis only depend on the ratio of $\sigma_{brain}/\sigma_{skull}$, or actually, does it depend on the individual values of σ_{brain} and σ_{skull}?

The real situation can be even more complicated with the sandwich-like substructure of the skull which contains two layers of compact bones with very low conductivity and one layer of spongiform tissue with higher conductivity (Leahy et al., 1998; Akhtari et al., 2003). If one treats the skull as a single layer, the effective conductivity of the skull may be inhomogeneous and anisotropic (Leahy et al., 1998). Furthermore, the effective conductivity of the scalp can also vary with skin conditions (e.g., bald, sweating), skin preparation procedures used for EEG, electrode contact sizes, and EEG gels and pastes. These factors raise two more questions that need consideration when integrating MEG and EEG data: 4): Will the results of an integrated approach be accurate if we model the complicated substructure of the skull with one layer of homogeneous and isotropic conductor? 5): If the conductivities of the scalp and brain are not the same, but are set equal in a model, will that arrangement affect the accuracy of the integrated MEG and EEG approach?

In the present study we addressed the above five key questions using computer simulations to test a new approach for combining simultaneously acquired MEG and EEG data, which uses a comprehensive analysis of the conductivity dependence to accurately derive the location and both the tangential and radial components of neuronal currents. In our approach, the source location and tangential components are first estimated from MEG alone, and the optimal combinations of conductivity values are obtained not only from best fitting to the EEG signal, but also by precisely matching the tangential components of sources from EEG to those from MEG. Then, the radial components of the source are obtained from EEG using the previously obtained optimal conductivity combinations. We hypothesized that: 1) A three-layered

conductor model with scalp, skull, and brain (the effective conductivity of the scalp equals that of the brain, i.e., $\sigma_{scalp} = \sigma_{brain}$), can adequately model a variety of conductivity distributions of the head including the substructure of the skull, the existence of the cerebrospinal fluid (CSF), and situations in which the $\sigma_{scalp} \neq \sigma_{brain}$; 2) There are non-unique, but well-organized combinations of the effective conductivity values for σ_{brain}, σ_{skull} and σ_{scalp} that can provide a virtually perfect fit to the integrated MEG and EEG data; 3) The radial component can be derived with high accuracy from the integrated MEG and EEG analysis without knowing the exact conductivity profile of the head tissue; 4) The integrated MEG and EEG approach works well for spherical head shape as well as for the more realistic head geometry; and 5) The integrated approach can provide accurate estimations of the parameters for single as well as multiple dipoles, even in the presence of realistic levels of measurement noise. Finally, we demonstrate the reliability of the performance of this new approach in an analysis of the 20-ms component of the simultaneously acquired human somatosensory evoked fields/potentials (SEFs/SEPs) elicited by electric median-nerve stimulation.

Material and Methods

EEG and MEG Head Models

A piece-wise homogeneous approximation was adopted in three-layered EEG and MEG head models (spherical or realistically-shaped model with BEM), in which the effective σ_{brain}, σ_{skull}, and σ_{scalp} need to be assigned. As we mentioned above, the effective σ_{brain} and σ_{scalp} cannot be determined independently from extracranial measures (an ill-posed problem), and are assumed to be the same ($\sigma_{scalp} = \sigma_{brain}$) as in most MEG and EEG studies. In our simulations, both a three-shell concentric spherical head model and a three-shell realistically-shaped BEM head model were examined. In the analysis of human SEFs/SEPs, the realistically-shaped BEM was applied. In both spherical and realistic head models, σ_{scalp} ($=\sigma_{brain}$) and σ_{skull} were varied independently and systematically to study their impact on the integrated MEG and EEG approach (see below).

The spherical MEG head model has a closed-form analytic solution, which is easy to compute (Cuffin and Cohen, 1977; Sarvas, 1987). The main feature of the spherical MEG model is its independence from the conductivity profile and the radius of the sphere which means that the calculation using Sarvas Formula does not change between single and multiple concentric spheres. At the limit, the Sarvas Formula holds even if the conductivity is zero (i.e. in the air). The single sphere EEG head model also has a closed-form analytic solution although here, the electric potential calculation depends on the conductivity and the radius of the sphere (Rush et al., 1969; Brody et al., 1973). The multi-shell concentric spherical EEG-forward calculation can be expressed analytically as an infinite series of Legendre polynomials, but it does not have a closed-form solution. On the other hand, the infinite series of Legendre polynomials can be approximated with some closed-form expressions (Ary et al., 1981; De Munck and Peters, 1993; Berg and Scherg, 1994; Zhang, 1995; Mosher et al., 1999). In the present study, the approach from Zhang (1995) and Mosher et al. (1999) was adopted.

Realistically-shaped EEG and MEG head models under the piece-wise homogeneous approximation can be solved by using the BEM (Meijs et al., 1987; Hamalainen and Sarvas, 1989; Ferguson et al., 1994; Schlitt et al., 1995; Mosher et al., 1999). With the BEM, each compartment of the head is assumed to be isotropic, with a constant conductivity value. The actual surfaces of the compartments (e.g. scalp, skull, and brain) are extracted from anatomical brain images of each subject (e.g., magnetic resonance (MR) or computed tomography (CT) images) and then tessellated into small triangles, i.e., boundary elements. To calculate the forward magnetic field or electric potential distributions using this realistic head model, one needs to make approximations regarding how the electric potentials vary across each triangle. The two common approximations are constant- and linear-potential approximations. In

addition, one needs to choose weighting functions to determine how to control the error across each triangle (Mosher et al., 1999). Two types of functions were studied: 1) The collocation method, which chooses the weighting function to be a Dirac delta function and controls the error at specific points of the triangles (center of mass, or the three vertices), and 2) The Galerkin method, which chooses the weighting function to be the same as the potential function, and controls the error in a global sense across each triangle. Thus, one usually ends up with four different types of BEMs, namely constant-collocation, linear-collocation, constant-Galerkin, and linear-Galerkin. Mosher and colleagues (Mosher et al., 1999) demonstrated that the linear-Galerkin method has the highest accuracy among the four, but the computational costs of Galerkin methods are extremely high, which greatly limits their practical applications in EEG and MEG analysis. In the present study, the realistic head model was based on the linear-collocation 3-layer BEM model and used for computer simulations and for analyzing human median nerve SEFs/SEPs.

Conductivity Dependence in Integrated Analysis of MEG and EEG Data

Several studies have shown that integrating MEG and EEG is more beneficial than using each modality alone (Baillet et al., 1999; Huizenga et al., 2001; Goncalves et al., 2003a; Babiloni et al., 2004). In the present study, we examined the conductivity dependence using a new integrated analysis of MEG and EEG data, for which the equivalent current dipole (ECD) model (Hamalainen et al., 1993) is adequate for both imaging modalities. The core of this approach is to first obtain the accurate source location information and the tangential components from conductivity-insensitive MEG first. Then this is integrated to obtain the radial component from the EEG data by adjusting the conductivity profile of the EEG model. The procedure for this integrated analysis is as follows:

I. Construct a spherical or realistically-shaped BEM head model for MEG, localize the neuronal source using non-linear optimization (i.e., down-hill simplex search for the source location parameters), and obtain the tangential components as well as the radial orientation of the source using MEG alone. Such calculations should be accurate, and either independent of the conductivity profile of the spherical head model, or insensitive to conductivity profile of the realistically-shaped BEM model.

II. Construct a piece-wise homogeneous three-shell concentric-spherical or realistically-shaped BEM head model (based on the surfaces of the scalp, outer skull, and inner skull from the MR images) for EEG. By varying σ_{brain} (which is set to be the same as σ_{scalp}) and σ_{skull} systematically and independently, we calculated the EEG forward gain matrices using the source location information from Step I.

III. Obtain the best fitting dipole moment parameters through a linear-fitting of the EEG data using the gain matrix from Step II for different conductivity values.

IV. Calculate the difference in tangential dipole moments between the ones obtained from EEG in Step III) for each combination of the σ_{brain} ($=\sigma_{scalp}$) and σ_{skull}, and the tangential components obtained from MEG in Step I to form a 2-D table. Then identify the optimal combinations of the σ_{brain} ($=\sigma_{scalp}$) and σ_{skull} that lead to the best match in tangential components between conductivity-sensitive EEG and conductivity-insensitive MEG. This is done using 2-D spline-interpolation and table looking-up. The goodness of fit of the tangential components obtained from EEG (a function of the conductivities) and the accurate tangential components from MEG (conductivity independent/insensitive) will be:

$$fit_{\text{tangential}} = \left(1 - \frac{\sum_{i=1}^{2} \left(p_i^{EEG}\left(\sigma_{scalp}, \sigma_{skull}\right) - p_i^{MEG} \right)^2}{\sum_{i=1}^{2} \left(p_i^{MEG} \right)^2} \right) \times 100\% \quad \text{(Eq. 1)}$$

where the summation in Eq. 1 is over the two tangential components.

V. With 2D spline-interpolation and table looking-up, identify the corresponding radial component from the EEG for which the optimal conductivity combinations were obtained in Step IV.

The basic principle of this new approach is to find the optimal conductivity profiles that best match the tangential components from the two modalities (i.e., MEG and EEG), and then obtain the radial component of the source from EEG using those optimal conductivity profiles.

Define the Radial Orientation using the MEG Gain Matrix

Identifying the radial orientation for a given dipole location in a spherical head model is trivial. However, defining the radial orientation may be a problem when using the realistically-shaped BEM head model. One method is to define the radial orientation by fitting the curvature of a portion of the inner skull surface near the source (local curvature fit) (e.g., (Leahy et al., 1998)). The problem, though, becomes how to define the term “local”. In the present study, we adopted a different approach wherein the optimal radial orientation was defined objectively and directly from the MEG gain matrix.

In this approach, for a given dipole location, an *N* by 3 MEG gain matrix is first calculated for a given MEG head model (spherical or realistically-shaped) where *N* is the number of MEG channels. Then, singular value decomposition (SVD) is performed for this gain matrix: $\mathbf{G} = \mathbf{USV}^{\mathbf{T}}$, and the radial orientation will be the singular vector in **V** that corresponds to the weakest singular value. In a spherical MEG model, the weakest singular value is precisely zero and the associated singular vector in **V** (in a null space) will be precisely the direction pointing from the center of the sphere to the dipole location. With the BEM model, the radial orientation obtained from the above procedure will be the orientation that is associated with the weakest singular value, which means that the dipole moment along that orientation will make the least-possible contribution to the MEG measurement (the one closest to the null space). Naturally, the two tangential orientations can be selected along the two singular vectors in **V** that are associated with the two stronger singular values. With the accurate radial orientation from MEG, we can decompose the total dipole moment from EEG into radial and tangential components. Note that the exact selection of the two tangential axes in our integrated analysis is not important since Eq. (1) is invariant to the selection of the two individual tangential orientations as long as they are both perpendicular to the radial orientation (i.e. invariant with respect to any rotation along the radial axis).

Computer Simulation Procedures

Six computer simulations were used to examine several key issues related to the conductivity profile of the head in the integrated MEG and EEG analysis using a piece-wise homogeneous, concentric spherical 3-shell head model, or 3-shell realistically-shaped BEM head model. These issues included: 1) With the assumption of the precise knowledge of the location of the dipole and the boundaries of the different compartments of the head tissue, is it enough to uniquely determine the $\sigma_{brain}/\sigma_{skull}$ ratio with EEG? 2) Can the new integrated MEG and EEG analysis accurately determine the radial components of the dipole moment? 3) Does the

accuracy of the integrated MEG and EEG analysis only depend on the ratio of $\sigma_{brain}/\sigma_{skull}$, or alternatively, does it depend on the individual values of σ_{brain} ($=\sigma_{scalp}$) and σ_{skull}? 4) Is the integrated approach using the piece-wise homogeneous three-shell head model sufficiently accurate when the actual conductivity profile contains a skull layer with two sub-layers of compact bones and a sub-layer of spongiform material, and when a layer of CSF is included in the simulation? 5) Does the integrated MEG and EEG approach work for both the concentric spherical head model and realistically-shaped BEM head model? 6) What is the performance of the integrated approach for multiple dipoles? And 7) What are the impacts of sensor noises and depths of the dipole on the results of the integrated MEG and EEG approach?

For spherical head models, the origin of the coordinate system was at the center of the concentric spheres. For the realistically-shaped BEM head models, three anatomical landmarks (i.e., left and right preauricular (PA), and nasion (NA)) were used to define the origin: The x-axis is defined as the direction from left-PA to right-PA, with positive x to the right direction; The y-axis is defined as a line through the NA intersecting and perpendicular to the left-right PA line, with positive y in the anterior direction. The z-axis is perpendicular to the x-y plane, with positive z in the superior direction. A three-layer realistically-shaped BEM head model was constructed with the surfaces of scalp, outer-skull, and inner-skull from the MR images. The number of triangles was 5120 for each surface.

In the MEG simulations, the sensor configuration from the whole-head Elekta Neuromag Oy VectorView™ MEG system (Helsinki, Finland) with 306 channels (204 planar gradiometer and 102 magnetometer channels) was adopted. For EEG, an EEG array with 61 pick-up electrodes uniformly distributed on the upper part of a spherical surface (scalp) was used. The locations of the MEG sensors and EEG electrodes are shown in Fig. 1(a) for the spherical head model, and in Fig. 1(b) for the realistically-shaped BEM head model.

Procedures for Integrated Analysis of Simultaneous Human MEG and EEG responses

The performance of our integrated MEG and EEG approach was further examined via analyzing the 20-ms component of simultaneously acquired SEFs/SEPs elicited by unilateral electric median-nerve stimulation. Such recordings have been routinely used in humans to study the somatosensory system, which is probably the most well-studied neuronal system in humans. Consequently, the underlying neuronal activity is well understood, which allowed us to predict with a high degree of confidence where sources should be found. Neurophysiological studies have shown that the electric stimulus dominantly activates the primary somatosensory area (SI) with a first component around 20 ms post-stimulus (Wood et al., 1985; Hari et al., 1993; Forss et al., 1994; Kawamura et al., 1996; Mauguiere et al., 1997a; Mauguiere et al., 1997b; Jousmaki and Forss, 1998; Forss and Jousmaki, 1998; Hari and Forss, 1999). The corresponding neuronal responses can be adequately modeled with a single dipole localized to Brodmann Area (BA) 3b. This test has been routinely used in clinical MEG exams and adopted previously in comparative and/or combined MEG and EEG analysis (Cohen and Cuffin, 1983; Goncalves et al., 2003a).

During the experiment, we conducted simultaneous MEG and EEG recordings from a healthy subject (41-years old, male) as he underwent electric median-nerve stimulation. The subject's right and left median-nerve were alternately stimulated using a bipolar Grass™ constant current stimulator (S88). The stimuli were square-wave electric pulses (0.2 ms duration) delivered at about 1 Hz (inter-stimulus interval: 800 ms to 1200 ms). The stimulus intensity was adjusted to 5 mA causing robust thumb twitches. A stimulus trigger from the stimulator was sent to the MEG acquisition system for signal averaging. SEFs/SEPs evoked by median-nerve stimulation were measured using the Elekta Neuromag Oy VectorView™ whole-head MEG system with 306 MEG channels (the same as the one used in simulations) and 64 EEG channels in an enhanced multi-layer magnetically shielded room (IMEDCO-AG, Switzerland) which

includes 3 layers of mu-metal, 3-layers of aluminum coated with gold at the junctions, plus one layer of active compensation (Cohen et al., 2002). The whole-head EEG electrode array contained 60 channels with unipolar silver-silver chloride electrodes (Elekta Neuromag Oy). EOG electrodes were used to detect eye blinks and eye movements. An interval of 500 ms post-stimulus was recorded, using 300 ms pre-stimulus data for noise estimation. Data were sampled at 1000 Hz and run through a high-pass filter with 0.1 Hz cut-off, a low-pass filter with 330 Hz cut-off, and through a notch filter (58–62 Hz) to remove 60 Hz power-line noise. Three hundred artifact-free MEG responses were averaged with respect to the stimulus trigger to increase the signal-to-noise ratio (SNR).

Structural MR images of the subject's head were collected using a General Electric 1.5T Excite MRI scanner (ver. 12 software release). Image acquisitions consisted of a pair of SPGR scans (TR=20ms, bandwidth=200Hz/pixel, FOV=25cm, matrix=256 × 192, slice thickness=1.33mm, 128 slices), using flip angles = 30° (T1-weighted) and 5° (PD-weighted). The T1-weighted images were used for superimposing MEG source locations. The PD-weighted images (co-registered with the T1) were used to obtain the innermost and outermost skull surfaces, as well as the scalp surface for the BEM head model (see below).

A three-layer realistically-shaped BEM head model was constructed with the surfaces of scalp, outer-skull, and inner-skull from the MR images. The number of triangles was 5120 for each surface. To co-register the MEG with MRI coordinate systems, the three anatomical landmarks (i.e., left and right PA, and NA) were measured for each subject using the Probe Position Identification system (Polhemus, USA). By identifying the same three points on the subject's MR images using Elekta Neuromag Oy VectorView™ software, a transformation matrix involving both rotation and translation between the MEG and MR coordinate systems was generated. To increase the reliability of the MEG-MR co-registration, approximately 80 points on the scalp were digitized with the Polhemus system, in addition to the three landmarks, to ensure that all points are located on the scalp surface of the MR images. Based on our experience, the MEG-MR co-registration error is expected to be less than 3 mm. The same subject-coordinate-system described in BEM simulations was also used in the analysis of the human median-nerve SEP/SEF.

Results

Simulation Case 0: Ill-posed Nature of the EEG Goodness-of-fit for Different Conductivities

This simulation examined how the goodness of fit of the EEG data changes with different combinations of σ_{brain} ($=\sigma_{scalp}$) and σ_{skull}. In this case, EEG and MEG data were generated from a dipole at location [−45.0, 7.2, 47.7] mm with dipole moments [6.0, 20.0, −18.0] nA•m (Cartesian coordinates) inside a three-layer concentric spherical head model with the center at the coordinate origin. The true tangential and radial dipole moments were 23.18 and 14.92 nA•m. The radii of the scalp, outer-skull, and brain were 88.0, 81.0, and 74.0 mm, respectively. The true conductivity values were set to be either [0.60, 0.01, and 0.60] (S/m) for scalp, skull, and brain, respectively, when the σ_{scalp} ($=\sigma_{brain}$)/σ_{skull} = 60, or [0.20, 0.01, and 0.20] (S/m) when the σ_{scalp} ($=\sigma_{brain}$)/σ_{skull} = 20. For the spherical head model, the EEG potentials and MEG fields can be calculated analytically. For EEG, the forward calculation depends on the conductivity profile, the center of the sphere, and radii of the concentric spheres (Zhang, 1995; Mosher et al., 1999), whereas for MEG, the forward calculations are conductivity-independent and depend only on the center of the sphere (Sarvas, 1987).

In this simulated case with concentric spheres, the MEG precisely localizes the dipole and the MEG result is independent of the conductivity profile. Taking the dipole location from the MEG (in this case it is the same as the 'ground truth'), we performed a linear fit to the EEG data for different combinations of σ_{brain} ($=\sigma_{scalp}$) and σ_{skull}. Fig. 2(a) shows the percent

variance of the fit, between the EEG potentials at the 61 electrodes generated by the true conductivity values, and the ones generated from different combinations of the σ_{scalp} ($=\sigma_{brain}$) and σ_{skull}. The dashed line in the plot is associated with the ground truth of σ_{scalp} ($=\sigma_{brain}$)/σ_{skull} = 60 with 100% fit. In addition, the contour lines shows that other conductivity combinations can fit the EEG data almost equally well (> 97% variance fit), with the exception of regions that have extremely low or extremely high σ_{scalp} ($=\sigma_{brain}$)/σ_{skull} ratios. In Fig. 2(b), a similar result was obtained when the true conductivity ratio of σ_{scalp} ($=\sigma_{brain}$)/σ_{skull} = 20, and the only difference was the slope of the contour lines. If a realistic amount of noise (e.g., 5%–10%) were added to the data, the percent variance fit would be indistinguishable between the one using the true conductivity values and other alternative conductivity combinations in a wide range (an ill-posed problem). This result indicates that it will be difficult to uniquely determine the conductivity ratio with EEG data alone, even if the source location is known.

Furthermore, unlike the conductivity-independent tangential dipole moments obtained from MEG, the tangential moments obtained from EEG alone showed orders of magnitudes of variations from ~0 nA•m to 912 nA•m for different conductivity combinations in the first example above with the truth σ_{scalp} ($=\sigma_{brain}$)/σ_{skull} = 60. Similarly, the radial moments from EEG changed from ~0 nA•m to 1364 nA•m as the conductivities varied. In the second example above with the truth σ_{scalp} ($=\sigma_{brain}$)/σ_{skull} = 20, the dipole components from EEG showed even larger variations when the conductivities changed, namely ~0 nA•m to 6607 nA•m for tangential and ~0 nA•m to 4546 nA•m for the radial components. Such large variations of dipole moments in EEG emphasized the need for an accurate method to obtain the tangential and radial dipole moments in our integrated MEG and EEG approach (see details in the following sections).

Simulation Case 1: Conductivity Dependence of the Integrated MEG and EEG Approach, Concentric Spheres, Homogeneous skull, $\sigma_{brain} = \sigma_{scalp}$, No Sensor Noise

This simulation examines the performance of our integrated MEG and EEG method in a three-layered concentric spherical model when the true conductivity values were set to be [0.30, 0.01, and 0.30] (S/m) for σ_{scalp}, σ_{skull}, and σ_{brain} respectively, and the conductivity values of the brain and scalp were equal. The other parameters (i.e., dipole location, dipole moments, and the radii of the three concentric spheres) were the same as in Case 0. We followed the 5 steps (I to V) listed in the Methods Section. Here, we use MEG to precisely obtain the dipole location and the tangential components of the dipole moments since the MEG solution is independent of the conductivity profile for the spherical head model. As described above, the two tangential orientations and the one radial orientation can be obtained directly from the MEG gain matrix, which is precisely rank-two in this case. The true dipole moments along the tangential and radial orientation were 23.18 and 14.92 nA•m, respectively (Table 1, under Case 1). Of course, one does not have to use the MEG gain matrix to determine the radial and tangential orientations in the spherical head models, but for realistic head-shape it can be crucial (see simulations with realistically-shaped BEM head model).

Applying now the integrated MEG and EEG analysis, we first obtained the accurate dipole location and tangential dipole moment from MEG (Table 1) -- neither the location nor the tangential moment showed any variations (indicated by zero standard deviations for these parameters, SD = 0) when the conductivities changed. In contrast, the tangential components from EEG can change several orders of magnitudes (not shown in the table) when the conductivity values vary in the ranges specified below. Then, we identified the conductivity combinations that led to a good match between the tangential components obtained from EEG (change with conductivities) and the accurate tangential components obtained from MEG (conductivity independent for spherical head) using Eq. 1. The fit of the tangential components across the two modalities is plotted for different combinations of σ_{scalp} ($=\sigma_{brain}$) and σ_{skull} in

Fig. 3(a). For each different testing conductivity profile, the values of σ_{scalp} (σ_{brain}) varied from 0.02 to 1.0 S/m at increments of 0.02 S/m, whereas the values of σ_{skull} varied from 0.005 to 0.03 S/m at increments of 0.0005 S/m. The best fitting line (>99% fit, dark-red color scale, using 2D-spline interpolation) is indicated with the solid black line in the plot. It is clear that for any given σ_{skull}, there is a unique σ_{scalp} ($=\sigma_{brain}$) value that leads to an accurate fit of the tangential components between EEG and MEG.

The key question now is whether the same combinations of σ_{scalp} ($=\sigma_{brain}$) and σ_{skull} that are associated with the best-fitting tangential components can also lead to an accurate measurement of the radial dipole moment. Fig. 3(b) plots the radial dipole moment (strength in color scale) for different combinations of σ_{scalp} ($=\sigma_{brain}$) and σ_{skull}. The solid black line is exactly the same conductivity combinations as the one in Fig. 3(a). Note that along this line, the color scales of the radial dipole moments remain virtually the same (i.e., green). The mean radial dipole moment and its variations with respect to the conductivity values along the solid black line was 14.82 ± 0.30 nA•m, which is nearly the same as ground truth of the radial dipole moment 14.92 nA•m. The small difference was due to the 2D-spline interpolation effect. This result shows that if we find the optimal conductivity combination associated with a good match of the tangential components between MEG and EEG, the same optimal conductivity combination will also lead to an accurate estimation of the radial dipole moment. In another words, our integrated MEG and EEG analysis can accurately estimate not only the dipole location but also all dipole moments (i.e., tangential and radial moments).

Unlike the conductivity dependence of the goodness-of-fit using solely EEG data (Fig. 2), the good match of the tangential components of integrated MEG and EEG analysis in Fig. 3(a)(b) is *not* ill-posed. Namely, for a given value of the σ_{skull}, the goodness-fit function is quite steep around the best corresponding value for the σ_{scalp} ($=\sigma_{brain}$). Another interesting finding is that the optimal conductivity combination (solid black line in Fig. 3(a)(b)) does not form a straight line passing through the origin. Although it appears that part of the optimal combination curve at the high end of the σ_{skull} values can be approximated as straight lines, the approximated straight lines do NOT pass the origin. Instead the y-intersect varies from point to point. This indicates that the integrated MEG and EEG analysis does not depend solely on the ratio of σ_{scalp} ($=\sigma_{brain}$)/σ_{skull}, rather it depends on both conductivity values in a well-organized fashion (i.e., along the solid black line).

Simulation Case 2: Concentric Spheres, Homogeneous skull, $\sigma_{brain} \neq \sigma_{scalp}$, No Sensor Noise

Next we examined the performance of our integrated MEG and EEG analysis for the situation in which the conductivities of the scalp and the brain were actually not the same ($\sigma_{scalp} \neq \sigma_{brain}$), contrary to the assumption of our EEG model. In this simulation study, the true dipole location and dipole moments, and the radii of the spherical scalp, outer-skull, and brain were the same as the ones used in Case 1. The only difference was that the true σ_{scalp}, σ_{skull}, and σ_{brain} were 0.60, 0.01, and 0.30 S/m respectively, with the conductivity of the scalp layer being twice as large as that of the brain to mimic the effective conductivity change of the skin due to skin conditions (e.g., bald, sweating, etc), EEG skin preparation procedures, electrode contact sizes, and EEG gels and pastes.

The same 5 steps of the integrated MEG and EEG analysis were followed and the results are shown in Fig. 3(c)(d) and in Table 1 (under Case 2). Again, the dipole location and tangential dipole moment were accurately obtained from MEG and neither of these parameters depended on the conductivity profile for the spherical head (Table 1). Fig. 3(c) shows that our model in which $\sigma_{scalp} = \sigma_{brain}$ can lead to close fits between the tangential components of the conductivity-dependent EEG and those from conductivity-independent MEG, even though the true σ_{scalp} is twice as large as the true σ_{brain}. The best fitting value along the solid black line (indicating the optimal conductivity combinations) in Fig. 3(c) was above 99% fit (2D-spline

interpolation). Fig 3(d) and Table 1 (under Case 2) show that along the line where the effective conductivity values lead to best fitting tangential dipole moments between MEG and EEG, the radial dipole moment was also accurately obtained (14.78 ± 0.29 nA•m).

Simulation Case 3: Concentric Spheres, Inhomogeneous and Anisotropic Skull, A layer of CSF, and $\sigma_{brain} \neq \sigma_{scalp}$, No Sensor Noise

A more challenging test of our integrated MEG and EEG approach are situations when substructures of the skull contain two layers of compact bones with very low conductivity and one layer of spongiform with higher conductivity. Effectively, the skull shows inhomogeneous and anisotropic properties in this situation (Leahy et al., 1998; Akhtari et al., 2003). We also included a layer CSF, and assigned different conductivity values to the scalp and skull as we did for Case 2 when we created the ground truth of the MEG and EEG signal. The purpose of this simulation was to see how our integrated MEG and EEG analysis using the simplified 3-layer piece-wise homogeneous EEG model with $\sigma_{scalp} = \sigma_{brain}$ behaves in a complicated situation such as this.

The simulated EEG signal was created with the same dipole parameters used in Cases 1 and 2, but with a 6-layer concentric spherical model that included the surfaces of the scalp, upper compact bone, spongiform, lower compact bone, CSF, and the brain. The radii of these surfaces were 88.0, 81.0, 79.0, 77.0, 75.0, and 74.0 mm, respectively. The conductivity values for this 6-layer model were 0.66, 0.007, 0.02, 0.007, 1.0, and 0.33 S/m. The conductivity values of the compact bones and spongiform layer of the skull were taken from the range of measurements reported in a study using fresh human skull segments in patients undergoing brain surgery (Akhtari et al., 2003).

The same 5-step integrated MEG and EEG analysis was conducted and the results are shown in Fig. 3(e)(f) and in Table 1. Although the true EEG signal was created by the more complicated 6-layer model, Fig. 3(e) shows that our integrated MEG and EEG analysis using the simplified 3-layer piece-wise homogeneous EEG model with equal conductivities for scalp and brain can generate accurate fits to the tangential dipole moments between the ones from the conductivity-dependent EEG and the precise ones from conductivity-independent MEG for a spherical head. The best fitting value along the solid black line (indicating the optimal conductivity combinations) in Fig. 3(e) was above 99.5% fit (2D-spline interpolation). Fig 3 (f) and Table 1 (under Case 3) show that along the line where the effective conductivity values led to best-fitting tangential dipole moments between MEG and EEG, the radial dipole moment was also accurately obtained (14.61 ± 0.30 nA•m).

Simulation Case 4: Realistic-head-shape, BEM, No Sensor Noise

In the previous simulations, concentric spherical EEG and MEG models were used. Next, we examined the performance of our integrated MEG and EEG approach using a realistically-shaped BEM head model. The BEM model was a piece-wise homogeneous 3-layer model containing outer-scalp, outer-skull, and inner-skull surfaces from a subject's MR images. The number of triangles was 5120 for each surface. In this simulation, 61-channel EEG and 306-channel MEG data were generated from a dipole at location [45.0, 17.2, 90.7] mm with dipole moments [−6.0, 20.0, −18.0] nA•m in subject-coordinate-system as determined by Left-PA, NA, and Right-PA. The true conductivity values were set to be [0.30, 0.01, and 0.30] S/m for scalp, skull, and brain, respectively. Using the SVD-based analysis, we can obtain the radial orientation [0.64, 0.28, 0.72] as the singular vector associated with the weakest singular value from the MEG gain matrix (see Method) and consequently, the decompose the true tangential and radial dipole moments at 23.22 nA•m and 14.86 nA•m, respectively

In our integrated MEG and EEG approach, the values of σ_{scalp} ($=\sigma_{brain}$) varied from 0.1 to 1.0 S/m at increments of 0.1 S/m, whereas the values of σ_{skull} varied from 0.001 to 0.015 S/m at increments of 0.001 S/m. Table 1 (under Case 4) lists the accuracy of the dipole location and tangential moment obtained using MEG, with mean and SD indicating the variations of these parameters across all combinations of the σ_{scalp} ($=\sigma_{brain}$) and σ_{skull}. The small SD values show that the MEG can accurately obtain the location and tangential moment of the dipole and the results were insensitive to the conductivity profile for read-head shape, very similar to the spherical head in which these parameters were totally independent of the conductivity profile. We also calculated the angle between the radial orientation associated with the true conductivity profile, and the ones for all testing conductivity profiles. The results ranged from 0° to 3.0° (mean 0.8° ± 0.6°) indicate that radial orientation is accurately obtained from MEG and it is insensitive to the conductivity profile of the realistically-shaped BEM head model.

Fig. 4(a)(b) show that our integrated MEG and EEG approach works well for a realistically-shaped BEM model. The approach can generate accurate fits to the tangential dipole moments between the ones from the conductivity-dependent EEG and the accurate ones from conductivity-insensitive MEG. The best fitting value of the tangential dipole moment along the solid black line (indicating the optimal conductivity combinations) in Fig. 4(a) was above 99% fit (2D-spline interpolation). Fig 4(b) and Table 1 (under Case 4) show that along the line where the effective conductivity values lead to best-fitting tangential dipole moments between MEG and EEG, the radial dipole moment was also accurately obtained (15.00 ± 0.25 nA•m), compared with true radial moment of 14.86 nA•m.

Simulation Case 5: Realistic Head-shape, BEM, Two-dipoles, No Sensor Noise

In the first part of this section, we examine the integrated MEG and EEG approach for two dipolar sources. The location of these two dipoles were [45.0, 17.2, 90.7] mm and [−58.0, 28.9, 54.0] mm, with dipole moments of [−6, 20, 18] nA•m and [17, 5, −19] nA•m, respectively. The conductivity profile, head geometry, and sensor configurations were the same as in Case 4. Using the SVD-based analysis of the MEG gain matrices, we obtained the true tangential and radial dipole moments for these two dipoles (Table 1).

Next, we varied the conductivity values of σ_{scalp} ($=\sigma_{brain}$) and σ_{skull}, the same way as we did in Case 4. For each conductivity combination, we localized the two dipoles using a down-hill simplex search and obtained their tangential dipole moments using MEG. The results in Table 1 show that these parameters were accurately obtained, with their variations across all conductivity profiles under testing similar to those in the one-dipole case (i.e., Case 4).

Fig. 5(c)–(f) show that the integrated MEG and EEG approach accurately obtained the radial components for both dipoles with a realistically-shaped BEM model, very similar to the one-dipole BEM case. For both dipoles, Table 1 (under Case 5a) lists the fitted radial dipole moments and their variations (SD) along optimal conductivity combinations (solid black lines in Fig. 5) for which the effective conductivity values lead to best-fitting tangential dipole moments between MEG and EEG.

Finally, we repeated the above MEG-EEG analysis for the two-dipole realistically-shaped BEM situation, but replaced the true σ_{scalp}, σ_{skull}, and σ_{brain} with [0.60, 0.01, and 0.30] S/m, respectively. The objective was to examine our model's performance for the situation in which the true conductivities of the scalp and the brain were not the same ($\sigma_{scalp} \neq \sigma_{brain}$), contrary to the assumption made in our model. The result in Table 1 (under Case 5b) shows that the locations and tangential moments of both dipoles were adequately obtained using MEG. The results for the radial moments of the two dipoles were also good using the MEG-EEG integration, and the modeling errors and variations were only slightly larger than those in the previous example by a few percent. This simulation demonstrated that our integrated MEG

and EEG approach is robust for a two-dipole realistically-shaped head model, and can still provide adequate results even when our model's assumption of $\sigma_{scalp} = \sigma_{brain}$ is violated.

Simulation Case 6: the Impacts of the Sensor Noise and Dipole Depth

Thus far, all simulations were performed without adding noise to either MEG or EEG sensors. In this section, we examined the performance of the integrated MEG and EEG approach by adding different levels of white Gaussian noise to both the MEG and EEG sensors, and by placing a dipole at either a cortical or a subcortical location. The noise-less MEG and EEG signal were calculated using the same 6-layer concentric spherical model used in Case 3, which included the scalp, upper compact bone, spongiform, lower compact bone, CSF, and brain. After noise was added, the analysis used the simplified 3-layer piece-wise homogeneous spherical model with $\sigma_{scalp} = \sigma_{brain}$.

The results from previous simulations showed that, for any given value of the σ_{skull}, there was a unique value for σ_{scalp} ($= \sigma_{brain}$), which leads to an accurate match and tangential dipole moments between MEG and EEG. This optimal conductivity combination also results in an accurate estimation of the radial dipole moment. Base on these findings, it is not necessary to analyze all combinations of the σ_{scalp} ($= \sigma_{brain}$) and σ_{skull}. Instead, we can simplify our calculation by arbitrarily fixing the σ_{skull} (say 0.01 S/m in this simulation) and only varying the σ_{scalp} ($= \sigma_{brain}$) in our model. Namely, we do not need to search for the entire solid black line for the optimal conductivity combinations every time, but rather look for one point on the curve. Note that our calculation can be simplified only after we have gone through the extensive analyses in previous examples.

Two noisy cases were studied. In the typical-noise case, the noise levels were assigned to mimic a typical evoked study corresponding to 100-trial averaging with SDs of the white Gaussian noises set at 8 fT/cm, 10 fT, and 0.38 μV for gradiometer MEG channels, magnetometer MEG channels, and EEG channels, respectively. In the high-noise case, the SDs of white noises were doubled, with respect to the typical-noise case (i.e., 16 fT/cm, 20 fT, and 0.76 μV). Monte-Carlo analyses were performed to assess the reliability of our method, in which 300 sets of different random noises with the same SDs (as listed above) were examined.

A single dipole was placed at two different depths to mimic cortical and deep subcortical generators. The coordinates of the cortical location were [−45.0 7.2, 47.7] mm and for the subcortical location, the coordinates were [−22.5 3.6, 23.8] mm, with the origin of the coordinate at the center of the concentric spheres. The dipole moments, namely [6, 20, −18] nA•m were the same for the single dipole at the two locations, with the tangential and radial orientation were 23.18 and 14.92 nA•m, respectively.

Table 2(a) lists the mean values and uncertainties of the fitted dipole location and tangential dipole moments obtained from MEG, and the radial dipole moments from MEG-EEG integration, for the cortical dipole under typical- and high-noise conditions. Please note that, as expected, when noise levels doubled, the uncertainties of the dipole parameters also approximately doubled. Fig. 5(a)–(d) plot the histograms of the tangential and radial dipole moments parameters for the cortical dipole source at different noise conditions. Even for the high-noise case, the estimations of these parameters were still reasonably good. For example, the uncertainties were 8% of the true value for the tangential moment, and ~20% for the radial moment. Note here the uncertainties, as measured by SDs across the 300 sets of random noises in the Monte-Carlo analysis, were mainly due to the added sensor noises, which should not be confused with the SDs in Table 1 where the variations across different conductivity profiles were studied.

Fig. 5(e)–(h) show the histograms of the tangential and radial moments obtained from the integrated MEG-EEG analysis for the deep subcortical dipole. Large uncertainties were observed for both the tangential and radial dipole moments, particularly for the high-noise case. The fitted values for the dipole location, tangential, as well as radial dipole moments are listed in the lower portion of Table 2(b). In the typical-noise case, the location uncertainties for this deep dipole were a few millimeters in all directions; the uncertainties were about 18% for the tangential moment and above 30% for the radial dipole moment. These uncertainties were nearly doubled for the high-noise case, although the mean values for all dipole parameters were still adequate.

Applying the Integrated MEG and EEG Analysis to Human Median-nerve Responses

The integrated MEG and EEG analysis was applied to two data sets in which we recorded simultaneous MEG and EEG responses evoked by unilateral (left or right) median-nerve stimulation in a healthy subject. The same 5-step integrated MEG and EEG analysis was applied to analyze the data. First, we localized a single dipole for the 20-ms component of the averaged SEF/SEP over three hundred artifact-free single-trials, elicited with electric median nerve stimulus, using MEG with a piece-wise homogeneous 3-layer realistically-shaped BEM head model containing outer-scalp, outer-skull, and inner-skull surfaces from the subject's MR images. The location of the neuronal source to right median nerve stimulus was in the left (contralateral) SI cortex in BA 3b, as illustrated with a dot in Fig. 6. Similarly, the stimulation of the left median nerve stimulation resulted in a source in the right SI cortex.

The second row of Table 3 shows the mean and SD of the dipole locations when we varied the conductivity value of the σ_{scalp} (σ_{brain}) in the range of 0.1–1.0 S/m and the σ_{skull} in the range of 0.001–0.015 S/m for the realistically-shaped head model. It is clear that the dipole locations (SD < 1mm in all directions) from MEG for either right or left SI dipole were highly insensitive to the conductivity profile.

Next, using the accurate dipole locations from MEG, we defined the radial orientation based on the SVD and obtained the tangential dipole moments for the SI sources: To demonstrate that the tangential components from MEG are insensitive to the conductivity profile, we also varied the conductivity values and found that the MEG gain matrices associated with different conductivity combinations were all highly rank-two matrices, from which we can robustly obtained the tangential component and the radial orientation; the results are listed in the Table 3.

Finally we varied the conductivity values in the 3-layer EEG BEM model to fit the EEG data, and detected the optimal combinations of $\sigma_{scalp}(=\sigma_{brain})$ and σ_{skull} that led to the best-fit of the tangential components between the ones obtained from the conductivity-dependent EEG and the accurate ones from conductivity-independent MEG, using the same methods as in the simulations. For the left SI dipole evoked by contralateral (right) median-nerve stimuli, the solid black line in Fig. 7(a) indicates the goodness-of-fit of the tangential components between MEG and EEG (> 98%). The same solid black line is also plotted in Fig. 7(b) which shows the radial dipole moment as a function of $\sigma_{scalp}(=\sigma_{brain})$ and σ_{skull}. The color scale indicates that the radial component from this integrated MEG and EEG analysis stays virtually the same along the solid black line (optimal conductivity combinations). The actual value of the radial dipole moment for this left SI dipole is listed in Table 3 (i.e., 13.6 ± 0.8 nA•m). Similarly, for right SI dipole evoked by left median-nerve stimuli, the solid black line in Fig. 7(c) shows the optimal conductivity combinations that were associated with the best match of the tangential components between MEG and EEG (> 96%). Along the same line, robust estimation of the radial component of the dipole was obtained (Fig. 7(d)) and the value is listed in Table 3 (i.e., −7.0 ± 0.4 nA•m). Note that the negative sign was ignored in the plot of Fig. 7(d) for the convenience of displaying the results.

Next, we have examined the conductivity-dependent variations of the dipole parameters (locations, tangential, and radial moments). To assess the reliability of the estimated dipole parameters for the left and right SI sources due to the existence of sensor- and brain-noises, we also performed a bootstrapping analysis (Efron, 1979) by re-sampling the three hundred single-trials with repetitions to form 1000 different sets of re-averaged data using the "BOOTSTRP" function in MATLAB. The advantage of the bootstrapping analysis is that it does not make specific assumptions about the statistical distribution of the noises (e.g., Gaussian white noise). Instead, it only requires that different single trials are independent. This requirement was easily fulfilled in our median-nerve exam since the sides of the stimuli (left/right) were randomized. The integrated MEG and EEG analysis was performed for each of the re-averaged data sets using the approach illustrated in simulation Case 6 by fixing σ_{skull} to be 0.01 S/m and only varying the σ_{scalp} (σ_{brain}). The mean values and uncertainties of the location, tangential, as well as the radial components of the left-SI and right-SI dipoles are listed in Table 3. The small uncertainty values indicate that these parameters were reliably estimated even in the presence of noise.

Computational cost of the BEM forward calculation

To effectively apply the integrated MEG and EEG approach to simulated and real data, the cost of the computation needs to be manageable. The main cost was from the forward MEG and EEG calculations when different conductivity profiles and/or different dipole locations were studied. This is not an issue for the spherical MEG and EEG models in which the forward calculations can be done rapidly with a typical desktop computer running MATLAB. The realistically-shaped head modeling using BEM, on the other hand, is more time consuming. For a given conductivity profile of the head, geometry, and MEG/EEG sensor configurations, one can construct the BEM transformation matrices (Mosher et al., 1999), and then the EEG and MEG forward calculation for a dipole can be computed in a fraction of a second. However, for each different combination of conductivity values, the MEG and EEG transformation matrices need to be recalculated (~24 minutes with our BEM mesh). The time-consuming BEM calculations of the MEG and EEG transformation matrices include: 1) construction of the system equations that involve the head geometry (~20 minutes for our BEM mesh) and the conductivity profile (negligible in computation time), and 2) the inversion of the EEG system matrix via LU decomposition and calculation of the MEG and EEG transformation matrices (~4 minutes). It is obvious that only the portion of the system equation associated with the conductivity profile needs to be updated in our integrated MEG and EEG approach. Unfortunately, the existing BEM code (Mosher et al., 1999) mixed the geometry and conductivity portions together when computing the system equation. In the present approach, we improved the BEM code by separating these two portions, and only updating the conductivity portion, for which the computation time was negligible (simple element-wise product). As a result, this improved BEM approach greatly reduced the analysis in the present study. Specifically, the total time to calculate the MEG and EEG transformation matrices was reduced to about 4 minutes when running MATLAB on a Dell 670 LINUX workstation with Xeon 3.0 GHz processor and 2 GB memory.

Discussion

We carried out an extensive analysis of the conductivity dependence using a new approach to combine simultaneous MEG and EEG data to accurately obtain not only the location and tangential component, but also the radial component of neuronal current. In our approach, the optimal effective conductivity values of the EEG model were derived from not only fitting the EEG signal, but also matching the tangential components from conductivity-dependent EEG to those from the conductivity-independent (spherical head) or conductivity-insensitive (realistic head) MEG. The results from computer simulations and analyses of human median-

nerve responses show that a three-layer conductor model with scalp, skull and brain ($\sigma_{scalp} = \sigma_{brain}$), can adequately model a variety of conductivity distributions of the head including the substructure of the skull (compact bones and spongiform material), the existence of the CSF layer, and the situation in which the conductivity of the scalp differs from that of the brain. One key finding was that our integrated MEG and EEG approach does not depend on the precise knowledge of the conductivity profile (see the right columns in Figs. 3, 4, and 7). In fact, one needs only the best conductivity combinations that both fit the EEG data and match the tangential components of the EEG and MEG (the solid black lines in Figs. 3, 4, and 7). Simulations and an application to human median-nerve stimulation responses also showed that our integrated analysis is sufficiently robust to realistic levels of sensor and brain noise, and works well for multiple dipoles as well as for a single dipole.

For a given σ_{skull} value in a reasonable range, one can find a unique value of σ_{scalp} ($=\sigma_{brain}$) that meets the requirement of the integrated MEG and EEG approach. However, because the slopes of the best conductivity combinations in Figs. 3, 4, and 7 were not constant, we found that one cannot uniquely determine the ratio of [σ_{scalp} ($=\sigma_{brain}$)/σ_{skull}] using the combined information from MEG and EEG. This finding can explain the dilemma surrounding the large discrepancy in conductivity ratios among previous studies using combined information from MEG and EEG. For example, one study reported a conductivity ratio of 80:1 (Cohen and Cuffin, 1983) and another reported a ratios between 43:1 to 86:1 (Goncalves et al., 2003a). We believe these discrepancies were simply due to which part of the optimal conductivity combination curve that previous studies fell into (i.e., the solid black lines in Figs. 3 and 5). If the skull conductivity was chosen to be near the low end, a higher ratio of σ_{scalp} ($=\sigma_{brain}$)/σ_{skull} will be needed to fit the integrated MEG and EEG data (i.e., large slope in the optimal conductivity combination line). In contrast, if one starts with the skull conductivity near the high end, a smaller ratio of σ_{scalp} ($=\sigma_{brain}$)/σ_{skull} will be observed (i.e., small slope in the optimal conductivity combination line). In another words, our results indicate that the debate about knowing the ratio of the σ_{scalp} ($=\sigma_{brain}$)/σ_{skull} should not be an issue any more for integrated MEG and EEG analyses, at least in our implementation.

Another finding of the present study was that the procedure for determining the conductivity profile by fitting EEG data alone is a highly ill-posed problem (see Fig. 2), even with precise knowledge of the source location and geometry of the head tissue, and under the assumption that $\sigma_{scalp} = \sigma_{brain}$ is precisely true. This is because with the amount of the noise in realistic measurements, there will be a wide range of conductivity values that can fit the EEG data essentially equally well. This is consistent with the large variation in the conductivities of the scalp (brain) and particularly the skull tissues reported in the literature, wherein brain conductivity ranges from 0.12 to 0.48 S/m (Nicholson, 1965;Goncalves et al., 2003a;Goncalves et al., 2003b), and of the human skull from 0.006 to 0.015 S/m (Geddes and Baker, 1967;Kosterich et al., 1983;Oostendorp et al., 2000;Goncalves et al., 2003a;Goncalves et al., 2003b). In contrast, our new integrated analysis with MEG and EEG is well-posed and it can accurately obtain all the source parameters without needing to know the precise conductivity profile.

We also introduced an objective way to obtain the optimal radial orientation for any dipole location as defined by the singular vector associated with the weakest singular value of the MEG gain matrix for a given head geometry. One advantage of this approach is that the radial orientation defined in this way is mathematically optimal because it generates the weakest possible MEG signal. Another advantage is that our approach is objective and does not depend on the subjective selection of the local curvature as traditional methods did. This is especially important for realistically-shaped head models such as the ones with BEM in which the phrase “radial orientation” is not as well-defined as it is for the spherical head. The most important issue here is to identify a dipole orientation that the MEG measurement is most insensitive to.

We continue to use the phase "radial orientation" or "radial components," but offer it an optimal definition based on SVD of the MEG gain matrix.

To work effectively, our integrated MEG and EEG approach requires that both MEG and EEG "see" the signal from the neuronal source. This makes sense since it would be meaningless to combine the information from both imaging modalities if the signal is missing in any individual modality. This requirement can be easily met with the majority of sources in the cortex. The human skull phantom study from Leahy and colleagues (Leahy et al., 1998) showed that dipoles with even small tangential components can still be accurately localized with MEG. One remaining concern is the "purely" radial oriented sources, for example, at the very bottom portion of the central sulcus in BA 3a. Fortunately, such source configurations appear to be rare, based on the detectability analysis from Hillebrand and Barnes (Hillebrand and Barnes, 2002).

There are substantial differences between our integrated MEG and EEG approach and ones from other studies. Fuchs and colleagues (Fuchs et al., 1998) proposed to scale the conductivity ratio of the EEG model by a common factor, in an attempt to achieve good fits for EEG and MEG data. To accomplish this goal, they required that in some latencies or latency ranges in the data, the MEG and EEG fields are generated by a single tangentially oriented dipole with negligible radial component. In a real example, they assumed that the median-nerve EEG and MEG responses were generated by a single tangentially oriented dipole and used it to scale the EEG data. Essentially, their method can be considered as a special case of our more generalized approach. In their special situation, the radial component plot in our integrated MEG and EEG approach would be zero for a spherical head shape model or nearly zero for a realistically-shaped head model. Specifically, the color scales would all be dark blue in the last columns of Figs. 3, 4, and 7. Our integrated MEG and EEG approach is more general and is designed to handle sources with not only tangential, but also non-zero radial components. Our method also works for multiple dipoles as well as for a single dipole. In reality, it is questionable if a purely tangential single dipole exists in real human neuronal responses, even for the median-nerve responses. There is no doubt that the median-nerve response at 20 ms latency is produced by a focal source with a strong tangential component. However, there is no guarantee in human anatomy that the shape of the posterior wall of the central sulcus will always orient in such a way that the radial component of the dipole becomes negligible. Out of curiosity, we analyzed the orientations of the posterior wall of the central sulcus (BA 3b) of the hand area in 5 subjects and found the orientations deviated from the tangential orientations (as defined by SVD of the MEG gain matrix) by 15° to as much as 56°. Even within the same subject, we observed large differences in orientations between left and right hand areas. More generally, it would seem that variability in cortical anatomy requires estimation of the non-zero radial components, such as those that we obtained using our integrated EEG and MEG approach in the present study (see Table 3 and Fig. 7).

In a separate study, Gutierrez and Nehorai (Gutierrez et al., 2004) applied maximum-likelihood and maximum a posteriori techniques to simultaneously estimate the layer conductivity ratios and source parameters using EEG data in a 4-layer concentric spherical EEG model with a single dipole, in which the location was obtained from either MEG or just EEG. However, for the simulated cases in which their approach worked well, the SNRs were set quite high (i.e., 53 dB and 80 dB). The requirement of a high SNR may not be met in empirical data. Such a result is to be expected, given the ill-posed nature of the goodness-of-fit for EEG with respect to different conductivity profiles as shown in Fig. 2 of the present study. Furthermore, their approach only provides the conductivity ratio(s), and this is not sufficient to accurate estimate the dipole moments – a key issue that our integrated EEG and MEG approach can address. In addition, it is not clear whether their approach can handle realistic head-shape or multiple dipoles as our approach can.

In the present study, a piece-wise homogenous approximation was adopted in a multi-shell concentric spherical model or a realistically-shaped BEM head model. To study the impact of local anisotropy of the conductivity distribution to the EEG and MEG forward calculation, the finite element method (FEM) should be considered. Recent FEM studies showed that the presence of local in-homogeneity and anisotropy of the conductivity in the tissue (particularly in the white matter) surrounding a deep source (i.e., at the thalamic level) substantially impacted both EEG and MEG forward calculations (Gencer and Acar, 2004; Wolters et al., 2005; Wolters et al., 2006). However, for sources at the cortical level, the influence of local in-homogeneity and anisotropy of the conductivity appeared to be much smaller than for deep sources. Gencer and Acar's study (Gencer and Acar, 2004) showed that at the cortical level, the sensitivities of MEG and EEG with respect to the local perturbation of conductivity drop by a factor of 10 at the size of one voxel for their FEM calculation, which is a few millimeters. Wolters and colleagues (Wolters et al., 2006) reported that the differences between anisotropic and isotropic white matter models were about 5% in both EEG and MEG when the anisotropy was assumed to be 10:1 in white matter, for either tangentially- or radially-oriented cortical sources. They also showed that the anisotropy of the skull had no impact on the MEG signal for tangentially oriented sources, whereas for EEG the impact was about 5% for either tangentially- or radially-oriented sources at the cortical level between isotropic and anisotropic models. The insensitivity of skull conductivity in MEG is consistent with our results using BEM, except our analyses were performed for a wide range of conductivity combinations. Importantly, another FEM study (Haueisen et al., 1995) found that the radially-oriented sources at either the cortical or deep level are very sensitive to the changes of the local conductivity, which motivated the present study to obtain the radial component of the source through an integrated MEG and EEG approach.

Studies using invasive methods have investigated the ratio of conductivities. For example, in vivo studies have estimated the conductivity of the skull. Lai and colleagues (Lai et al., 2005) used simultaneous extra- and intra-cranial potential recordings induced by subdural current stimulation to estimate the brain-to-skull conductivity ratio in 5 pediatric epilepsy patients (aged from 8 to 12 years of age) using a three-shell concentric volume conductor head model. They found the in vivo effective ratio ranged from 18 to 34. In another study (Akhtari et al., 2002), conductivity of the bulk skull, two compact-bone sub-layers of the skull, and the spongiform sub-layer were estimated from fresh skull pieces in the four neurosurgical patients of aged 17, 61, 75 and 75 years of age. Although the conductivities of the sub-layer of the skull showed large variations (i.e., 2.83—12.2 for the compact bone and 16.2—41.3 for the spongiform sub-layer), conductivity estimates of the bulk skull appeared more consistent across ages (i.e., 8.50—11.4). Still, the amount of inter-subject variation in invasive measurements is unclear due to the very small samples of studies. Moreover, the main problem is that just knowing the conductivity ratio is not sufficient to accurately determine either the tangential or radial components of the dipole with EEG alone (see simulation Case 0). The present study provides a non-invasive way of accurately estimating both dipole moments using an integrated MEG and EEG approach. Once the conductivities are set individually they can be used for any other MEG/EEG data set of the same individual increasing the accuracy of each brain imaging modality.

Acknowledgments

This work was supported in part by the Department of Radiology, University of California at San Diego, by four Merit Review Grants from the Department of Veterans Affairs (two for Huang, one for Lee, and one for Harrington), National Institute of Health Grants R01-NS18741 (Halgren), R01-NS44623 (Halgren), R01-EB00790 (Dale), R01-HD053136 (Elman), and by Kavli Institute for Brain and Mind (Elman). We would also like to thank two anonymous reviewers' constructive suggestions that substantially strengthen the present study

Reference List

Akhtari M, Bryant HC, Emin D, Merrifield W, Mamelak AN, Flynn ER, Shih JJ, Mandelkern M, Matlachov A, Ranken DM, Best ED, DiMauro MA, Lee RR, Sutherling WW. A model for frequency dependence of conductivities of the live human skull. Brain Topogr 2003;16:39–55. [PubMed: 14587968]

Akhtari M, Bryant HC, Mamelak AN, Flynn ER, Heller L, Shih JJ, Mandelkern M, Matlachov A, Ranken DM, Best ED, DiMauro MA, Lee RR, Sutherling WW. Conductivities of three-layer live human skull. Brain Topogr 2002;14:151–167. [PubMed: 12002346]

Ary JP, Darcey TM, Fender DH. A method for locating scalp electrodes in spherical coordinates. IEEE Trans Biomed Eng 1981;28:834–836. [PubMed: 7044949]

Babiloni F, Babiloni C, Carducci F, Romani GL, Rossini PM, Angelone LM, Cincotti F. Multimodal integration of EEG and MEG data: a simulation study with variable signal-to-noise ratio and number of sensors. Hum Brain Mapp 2004;22:52–62. [PubMed: 15083526]

Baillet S, Garnero L, Marin G, Hugonin JP. Combined MEG and EEG source imaging by minimization of mutual information. IEEE Trans Biomed Eng 1999;46:522–534. [PubMed: 10230131]

Barth DS, Sutherling W, Broffman J, Beatty J. Magnetic localization of a dipolar current source implanted in a sphere and a human cranium. Electroencephalogr Clin Neurophysiol 1986;63:260–273. [PubMed: 2419084]

Berg P, Scherg M. A fast method for forward computation of multiple-shell spherical head models. Electroencephalogr Clin Neurophysiol 1994;90:58–64. [PubMed: 7509274]

Brenner D, Lipton J, Kaufman L, Williamson SJ. Somatically evoked magnetic fields of the human brain. Science 1978;199:81–83. [PubMed: 17569490]

Brody DA, Terry FH, Ideker RE. Eccentric dipole in a spherical medium: generalized expression for surface potentials. IEEE Trans Biomed Eng 1973;20:141–143. [PubMed: 4688306]

Cohen D, Cuffin BN. Demonstration of useful differences between magnetoencephalogram and electroencephalogram. Electroencephalogr Clin Neurophysiol 1983;56:38–51. [PubMed: 6190632]

Cohen D, Cuffin BN. A method for combining MEG and EEG to determine the sources. Phys Med Biol 1987;32:85–89. [PubMed: 3823144]

Cohen, D.; Schläpfer, U.; Ahlfors, S.; Hämäläinen, M.; Halgren, E. In: Nowak, HHJ.; Gießler, F., editors. New Six-Layer Magnetically-Shielded Room for MEG; Proceedings of the 13th International Conference on Biomagnetism; Jena, Germany: VDE Verlag; 2002. p. 919-921.

Cuffin BN. EEG localization accuracy improvements using realistically shaped head models. IEEE Trans Biomed Eng 1996;43:299–303. [PubMed: 8682542]

Cuffin BN, Cohen D. Magnetic fields of a dipole in special volume conductor shapes. IEEE Trans Biomed Eng 1977;24:372–381. [PubMed: 881208]

Cuffin BN, Cohen D, Yunokuchi K, Maniewski R, Purcell C, Cosgrove GR, Ives J, Kennedy J, Schomer D. Tests of EEG localization accuracy using implanted sources in the human brain. Ann Neurol 1991;29:132–138. [PubMed: 2012383]

De Munck JC, Peters MJ. A fast method to compute the potential in the multisphere model. IEEE Trans Biomed Eng 1993;40:1166–1174. [PubMed: 8307601]

Efron B. 1977 Rietz Lecture - Bootstrap Methods - Another Look at the Jackknife. Annals of Statistics 1979;7:1–26.

Ferguson AS, Zhang X, Stroink G. A complete linear discretization for calculating the magnetic field using the boundary element method. IEEE Trans Biomed Eng 1994;41:455–460. [PubMed: 8070805]

Forss N, Hari R, Salmelin R, Ahonen A, Hamalainen M, Kajola M, Knuutila J, Simola J. Activation of the human posterior parietal cortex by median nerve stimulation. Exp Brain Res 1994;99:309–315. [PubMed: 7925811]

Forss N, Jousmaki V. Sensorimotor integration in human primary and secondary somatosensory cortices. Brain Res 1998;781:259–267. [PubMed: 9507157]

Fuchs M, Wagner M, Wischmann HA, Kohler T, Theissen A, Drenckhahn R, Buchner H. Improving source reconstructions by combining bioelectric and biomagnetic data. Electroencephalogr Clin Neurophysiol 1998;107:93–111. [PubMed: 9751281]

Geddes LA, Baker LE. The specific resistance of biological material--a compendium of data for the biomedical engineer and physiologist. Med Biol Eng 1967;5:271–293. [PubMed: 6068939]

Gencer NG, Acar CE. Sensitivity of EEG and MEG measurements to tissue conductivity. Phys Med Biol 2004;49:701–717. [PubMed: 15070197]

Goncalves S, De Munck JC, Verbunt JP, Heethaar RM, da Silva FH. In vivo measurement of the brain and skull resistivities using an EIT-based method and the combined analysis of SEF/SEP data. IEEE Trans Biomed Eng 2003a;50:1124–1128. [PubMed: 12943281]

Goncalves SI, De Munck JC, Verbunt JP, Bijma F, Heethaar RM, Lopes da SF. In vivo measurement of the brain and skull resistivities using an EIT-based method and realistic models for the head. IEEE Trans Biomed Eng 2003b;50:754–767. [PubMed: 12814242]

Gutierrez D, Nehorai A, Muravchik CH. Estimating brain conductivities and dipole source signals with EEG arrays. IEEE Trans Biomed Eng 2004;51:2113–2122. [PubMed: 15605858]

Hamalainen MS, Hari R, Ilmoniemi RJ, Knuutila J, Lounasmaa OV. Magnetoencephalography--theory, instrumentation, and applications to noninvasive studies of the working human brain. Reviews of Modern Physics 1993;65:413–497.

Hamalainen MS, Sarvas J. Realistic conductivity geometry model of the human head for interpretation of neuromagnetic data. IEEE Trans Biomed Eng 1989;36:165–171. [PubMed: 2917762]

Hansen JS, Ko HW, Fisher RS, Litt B. Practical limits on the biomagnetic inverse process determined from in vitro measurements in spherical conducting volumes. Phys Med Biol 1988;33:105–111. [PubMed: 3353445]

Hari R, Forss N. Magnetoencephalography in the study of human somatosensory cortical processing. Philos Trans R Soc Lond B Biol Sci 1999;354:1145–1154. [PubMed: 10466142]

Hari R, Karhu J, Hamalainen M, Knuutila J, Salonen O, Sams M, Vilkman V. Functional organization of the human first and second somatosensory cortices: a neuromagnetic study. Eur J Neurosci 1993;5:724–734. [PubMed: 8261143]

Haueisen J, Ramon C, Czapski P, Eiselt M. On the influence of volume currents and extended sources on neuromagnetic fields: a simulation study. Ann Biomed Eng 1995;23:728–739. [PubMed: 8572423]

Henderson CJ, Butler SR, Glass A. The localization of equivalent dipoles of EEG sources by the application of electrical field theory. Electroencephalogr Clin Neurophysiol 1975;39:117–130. [PubMed: 50209]

Hillebrand A, Barnes GR. A quantitative assessment of the sensitivity of whole-head MEG to activity in the adult human cortex. Neuroimage 2002;16:638–650. [PubMed: 12169249]

Huizenga HM, van Zuijen TL, Heslenfeld DJ, Molenaar PC. Simultaneous MEG and EEG source analysis. Phys Med Biol 2001;46:1737–1751. [PubMed: 11474922]

Janday BS, Swithenby SJ. Analysis of magnetoencephalographic data using the homogeneous sphere model: empirical tests. Phys Med Biol 1987;32:105–113. [PubMed: 3823128]

Jousmaki V, Forss N. Effects of stimulus intensity on signals from human somatosensory cortices. Neuroreport 1998;9:3427–3431. [PubMed: 9855293]

Kawamura T, Nakasato N, Seki K, Kanno A, Fujita S, Fujiwara S, Yoshimoto T. Neuromagnetic evidence of pre- and post-central cortical sources of somatosensory evoked responses. Electroencephalogr Clin Neurophysiol 1996;100:44–50. [PubMed: 8964262]

Kosterich JD, Foster KR, Pollack SR. Dielectric permittivity and electrical conductivity of fluid saturated bone. IEEE Trans Biomed Eng 1983;30:81–86. [PubMed: 6832795]

Krings T, Chiappa KH, Cuffin BN, Cochius JI, Connolly S, Cosgrove GR. Accuracy of EEG dipole source localization using implanted sources in the human brain. Clin Neurophysiol 1999;110:106–114. [PubMed: 10348329]

Lai Y, van DW, Ding L, Hecox KE, Towle VL, Frim DM, He B. Estimation of in vivo human brain-to-skull conductivity ratio from simultaneous extra- and intra-cranial electrical potential recordings. Clin Neurophysiol 2005;116:456–465. [PubMed: 15661122]

Leahy RM, Mosher JC, Spencer ME, Huang MX, Lewine JD. A study of dipole localization accuracy for MEG and EEG using a human skull phantom. Electroencephalogr Clin Neurophysiol 1998;107:159–173. [PubMed: 9751287]

Liu AK, Dale AM, Belliveau JW. Monte Carlo simulation studies of EEG and MEG localization accuracy. Hum Brain Mapp 2002;16:47–62. [PubMed: 11870926]

Mauguiere F, Merlet I, Forss N, Vanni S, Jousmaki V, Adeleine P, Hari R. Activation of a distributed somatosensory cortical network in the human brain. A dipole modelling study of magnetic fields evoked by median nerve stimulation Part I: Location and activation timing of SEF sources. Electroencephalogr Clin Neurophysiol 1997a;104:281–289. [PubMed: 9246065]

Mauguiere F, Merlet I, Forss N, Vanni S, Jousmaki V, Adeleine P, Hari R. Activation of a distributed somatosensory cortical network in the human brain: a dipole modelling study of magnetic fields evoked by median nerve stimulation. Part II: Effects of stimulus rate, attention and stimulus detection. Electroencephalogr Clin Neurophysiol 1997b;104:290–295. [PubMed: 9246066]

Meijs JW, Bosch FG, Peters MJ, Lopes da Silva FH. On the magnetic field distribution generated by a dipolar current source situated in a realistically shaped compartment model of the head. Electroencephalogr Clin Neurophysiol 1987;66:286–298. [PubMed: 2434313]

Mosher JC, Leahy RM, Lewis PS. EEG and MEG: forward solutions for inverse methods. IEEE Trans Biomed Eng 1999;46:245–259. [PubMed: 10097460]

Nicholson PW. Specific impedance of cerebral white matter. Exp Neurol 1965;13:386–401. [PubMed: 5847284]

Ollikainen JO, Vauhkonen M, Karjalainen PA, Kaipio JP. Effects of local skull inhomogeneities on EEG source estimation. Med Eng Phys 1999;21:143–154. [PubMed: 10468356]

Oostendorp TF, Delbeke J, Stegeman DF. The conductivity of the human skull: results of in vivo and in vitro measurements. IEEE Trans Biomed Eng 2000;47:1487–1492. [PubMed: 11077742]

Pohlmeier R, Buchner H, Knoll G, Rienacker A, Beckmann R, Pesch J. The influence of skull-conductivity misspecification on inverse source localization in realistically shaped finite element head models. Brain Topogr 1997;9:157–162. [PubMed: 9104826]

Rush S, Lepeschkin E, Gregoritsch A. Current distribution from defibrillation electrodes in a homogeneous torso model. J Electrocardiol 1969;2:331–341. [PubMed: 5382231]

Sarvas J. Basic mathematical and electromagnetic concepts of the biomagnetic inverse problem. Phys Med Biol 1987;32:11–22. [PubMed: 3823129]

Schlitt HA, Heller L, Aaron R, Best E, Ranken DM. Evaluation of boundary element methods for the EEG forward problem: effect of linear interpolation. IEEE Trans Biomed Eng 1995;42:52–58. [PubMed: 7851930]

Smith DB, Sidman RD, FLANIGIN H, Henke J, Labiner D. A reliable method for localizing deep intracranial sources of the EEG. Neurology 1985;35:1702–1707. [PubMed: 4069360]

Smith DB, Sidman RD, Henke JS, FLANIGIN H, Labiner D, Evans CN. Scalp and depth recordings of induced deep cerebral potentials. Electroencephalogr Clin Neurophysiol 1983;55:145–150. [PubMed: 6185310]

van den Broek SP, Reinders F, Donderwinkel M, Peters MJ. Volume conduction effects in EEG and MEG. Electroencephalogr Clin Neurophysiol 1998;106:522–534. [PubMed: 9741752]

Weinberg H, Brickett P, Coolsma F, Baff M. Magnetic localisation of intracranial dipoles: simulation with a physical model. Electroencephalogr Clin Neurophysiol 1986;64:159–170. [PubMed: 2424731]

Wolters, CH.; Anwander, A.; Tricoche, X.; Lew, S.; Johnson, CR. Influence of local and remote white matter conductivity anisotropy for a thalamic source on EEG/MEG field and return current computation. 7. 2005. p. 203-206.

Wolters CH, Anwander A, Tricoche X, Weinstein D, Koch MA, MacLeod RS. Influence of tissue conductivity anisotropy on EEG/MEG field and return current computation in a realistic head model: a simulation and visualization study using high-resolution finite element modeling. Neuroimage 2006;30:813–826. [PubMed: 16364662]

Wood CC, Cohen D, Cuffin BN, Yarita M, Allison T. Electrical sources in human somatosensory cortex: identification by combined magnetic and potential recordings. Science 1985;227:1051–1053. [PubMed: 3975600]

Yamamoto T, Williamson SJ, Kaufman L, Nicholson C, Llinas R. Magnetic localization of neuronal activity in the human brain. Proc Natl Acad Sci USA 1988;85:8732–8736. [PubMed: 3186757]

Zhang Z. A fast method to compute surface potentials generated by dipoles within multilayer anisotropic spheres. Phys Med Biol 1995;40:335–349. [PubMed: 7732066]

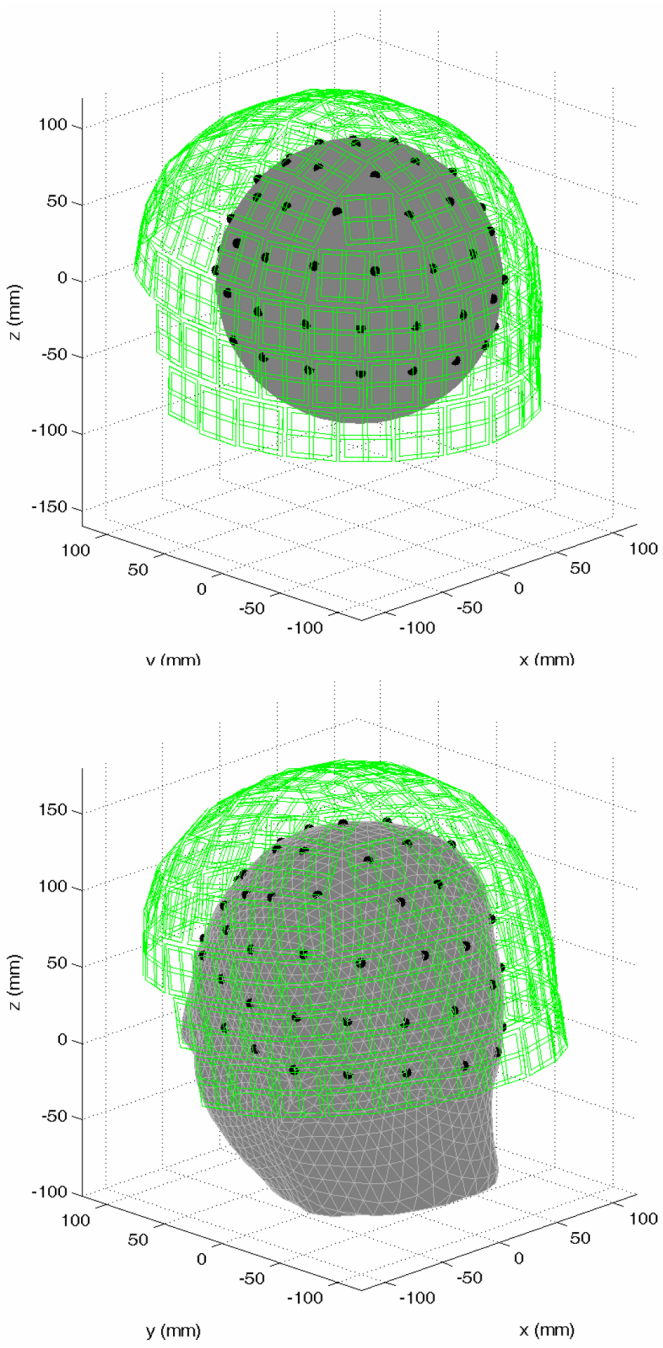

Figure 1.
The 306-channel Elekta Neuromag Vectorview™ MEG and 61-channel EEG sensor configurations used in the computer simulations for (a): Spherical head model where the coordinate origin is at the center of the concentric spheres, and (b): Realistically-shaped BEM head model where the origin of the subject-coordinate system is defined by left-PA, NA, and right-PA.

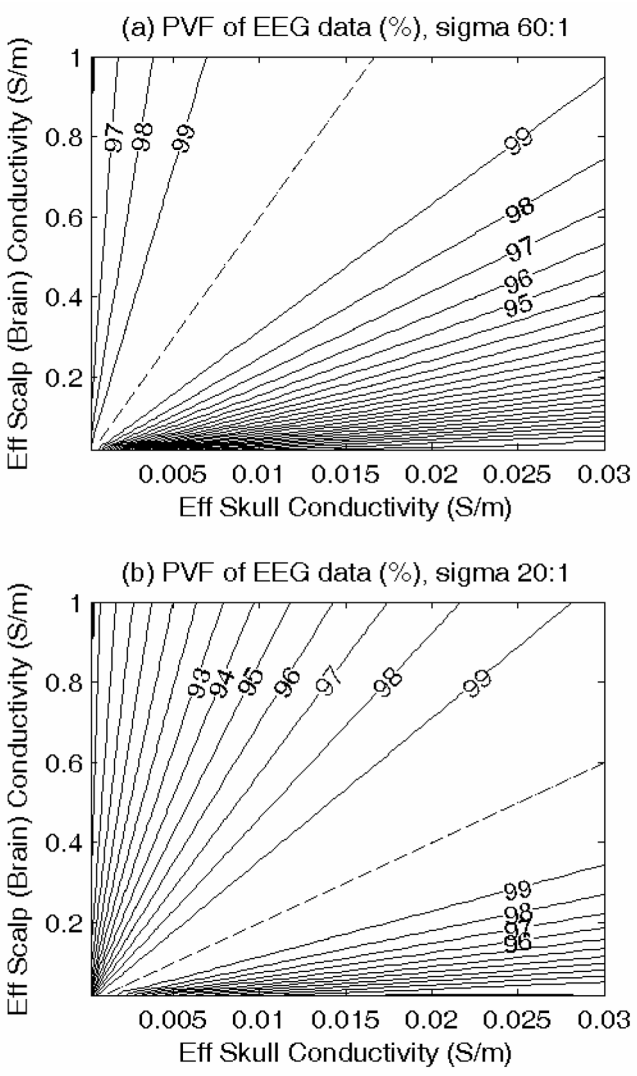

Figure 2.

Contour plots showing the goodness-of-fit (percent variance) of the EEG potentials with different combinations of the σ_{scalp} ($=\sigma_{brain}$) and σ_{skull}, for two values of conductivity ratios. (a) σ_{scalp} ($=\sigma_{brain}$)/σ_{skull} = 60. The dashed line in the plot is associated with the true conductivity ratio of 60 at 100% level. (b) σ_{scalp} ($=\sigma_{brain}$)/σ_{skull} = 20. The dashed line is for the true conductivity ratio of 20 at 100% goodness-of-fit level.

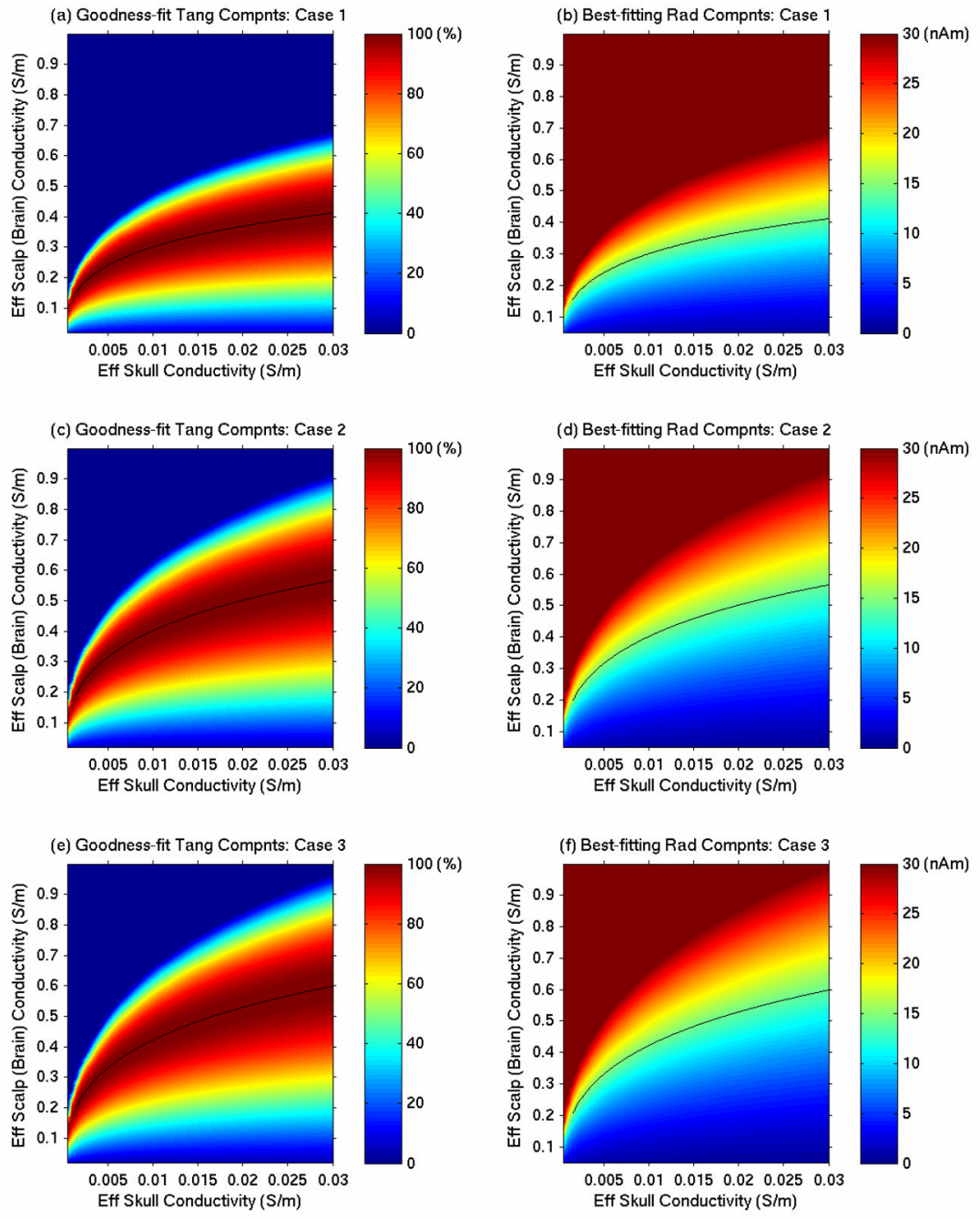

Figure 3.

Three computer simulation studies of conductivity dependence using the integrated MEG and EEG analysis for spherical head. Left column: Obtaining the optimal conductivity combinations in the EEG model that best matches the tangential components obtained from EEG and the accurate tangential components from MEG. The solid black lines indicate the optimal conductivity combinations. Right column: Reconstructed radial components obtained from the optimal conductivity combinations. (a) and (b): Case 1 in which the true conductivity values of the scalp and the brain were the same (homogenous skull, $\sigma_{scalp} = \sigma_{brain}$). (c) and (d): Case 2 in which the true scalp conductivity was twice as much as that of the brain (homogenous skull, $\sigma_{scalp} \neq \sigma_{brain}$). (e) and (f): Case 3 in which the true conductivity profile contains 6 layers

including the scalp, upper compact bone, spongiform, lower compact bone, CSF, and brain (inhomogeneous and anisotropic skull, a layer of CSF, and $\sigma_{brain} \neq \sigma_{scalp}$).

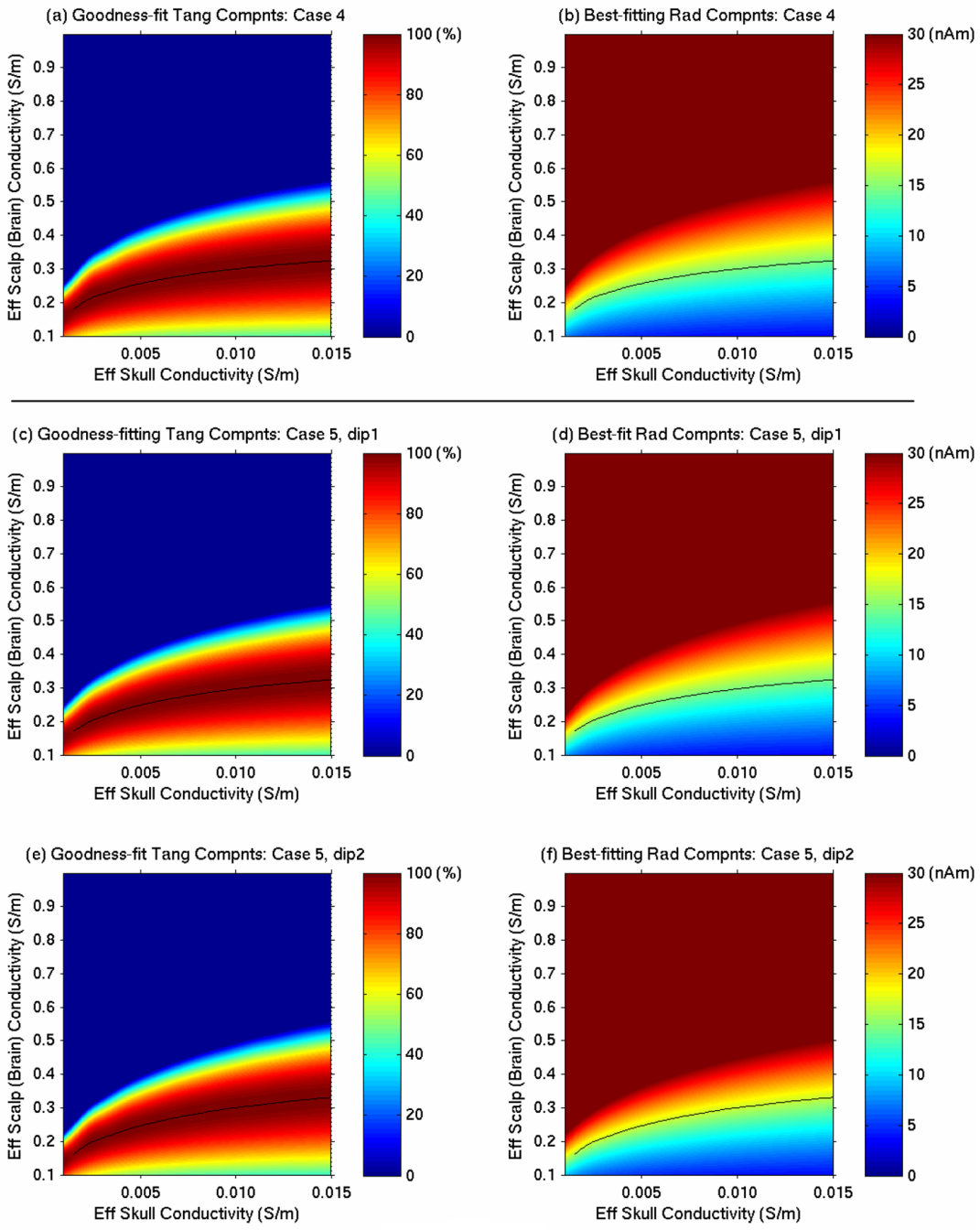

Figure 4.

Computer simulation studies of conductivity dependence using the integrated MEG and EEG analysis with realistically-shaped 3-shell BEM model, for 1 and 2 dipoles. The true conductivity values of the scalp and the brain were the same (homogenous skull, $\sigma_{scalp} = \sigma_{brain}$). The meanings of the color scales are the same as those in Fig. 4. Subplot (a) and (b): one-dipole Case 4. (c) and (d): dipole #1 of a two-dipole Case 5. (e) and (f): dipole #2 of the two-dipole Case 5.

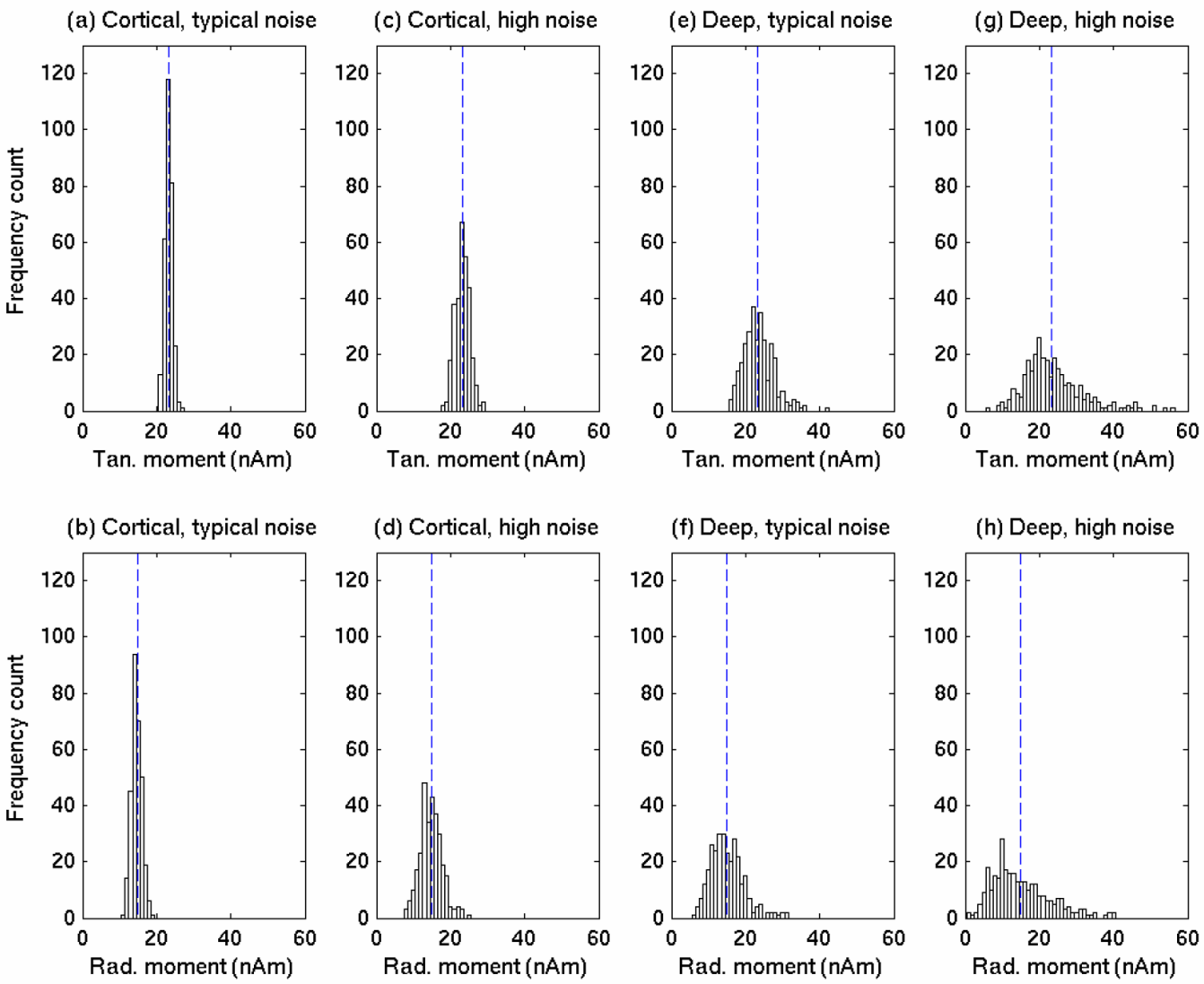

Figure 5.

Histogram plots showing the uncertainty of the dipole parameters using the integrated MEG and EEG approach when different levels of sensor noise are added and when a single dipole is placed at different depths.

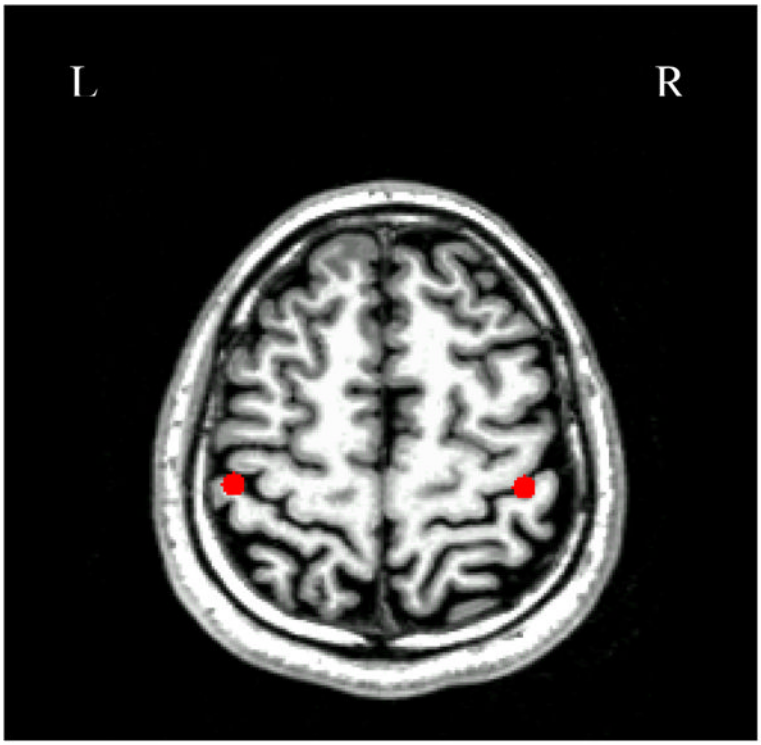

Figure 6.
Primary somatosensory dipoles in left and right BA 3b evoked by contralateral median-nerve stimulation. The localization was obtained by fitting the MEG data using a three-shell realistically-shaped BEM head model and the results were superimposed on the subject's MRI.

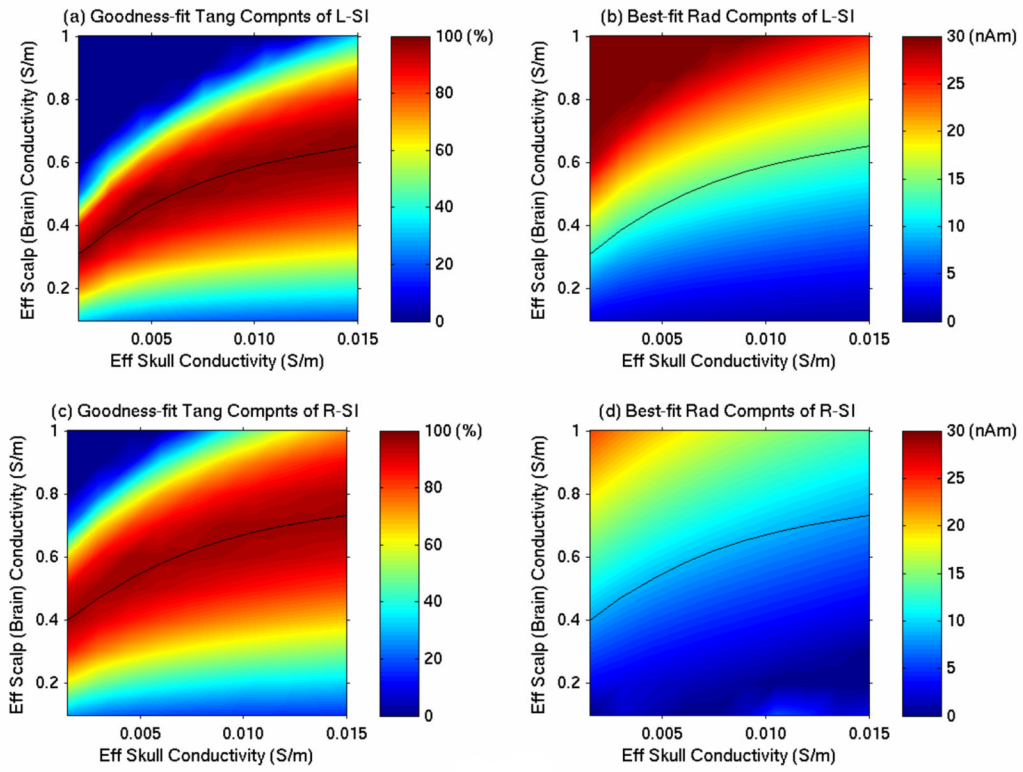

Figure 7.

Analysis of human median nerve responses using the integrated MEG and EEG approach. Left column: Obtaining the optimal conductivity combinations (solid black lines) in the EEG model that best match the tangential components obtained from EEG and the accurate tangential components from MEG. Right column: Reconstructed radial components obtained from the optimal conductivity combinations. (a) and (b): Left SI dipole evoked by right median-nerve stimulation. (c) and (d): Right SI dipole evoked by left median-nerve stimulation.

Table 1

Simulation results for the conductivity dependence of integrated MEG and EEG analysis. The results are listed for each of the five simulation cases. In each case, the two tangential axes and one radial axis were obtained from the SVD of the MEG gain matrix.

	True Values	Fitted Values (mean ± SD)
Case 1 (1-dipole, spherical)		
Location† [x, y, z] (mm):	[−45.0, 7.2, 47.7]	[−45.0, 7.2, 47.7] ± [0, 0, 0]
Tangential moment† (nAm):	23.18	23.18 ± 0.00
Radial moment‡ (nAm):	14.92	14.82 ± 0.30
Case 2 (1-dipole, spherical)		
Location† [x, y, z] (mm):	[−45.0, 7.2, 47.7]	[−45.0, 7.2, 47.7] ± [0, 0, 0]
Tangential moment† (nAm):	23.18	23.18 ± 0.00
Radial moment‡ (nAm):	14.92	14.78 ± 0.29
Case 3 (1-dipole, spherical)		
Location† [x, y, z] (mm):	[−45.0, 7.2, 47.7]	[−45.0, 7.2, 47.7] ± [0, 0, 0]
Tangential moment† (nAm):	23.18	23.18 ± 0.00
Radial moment‡ (nAm):	14.92	14.61 ± 0.30
Case 4 (1-dipole, BEM)		
Location† [x, y, z] (mm):	[45.0, 17.2, 90.7]	[44.8, 17.4, 90.3] ± [0.4, 0.3, 0.6]
Tangential moment† (nAm):	23.22	23.77 ± 0.57
Radial moment‡ (nAm):	14.86	14.99 ± 0.25
Case 5a (2-dipole, BEM), Dipole #1		
Location† [x, y, z] (mm):	[45.0, 17.2, 90.7]	[44.4, 17.4, 89.9] ± [0.6, 0.3, 0.8]
Tangential moment† (nAm):	23.22	24.08 ± 0.88
Radial moment‡ (nAm):	14.86	14.93 ± 0.49
Case 5a (2-dipole, BEM), Dipole #2		
Location† [x, y, z] (mm):	[−58.0, 28.9, 54.0]	[−57.5, 28.8, 54.0] ± [0.5, 0.2, 0.1]
Tangential moment† (nAm):	19.60	20.44 ± 0.92
Radial moment‡ (nAm):	17.05	16.99 ± 0.22
Case 5b (2-dipole, BEM), Dipole #1		
Location† [x, y, z] (mm):	[45.0, 17.2, 90.7]	[43.9, 17.5, 89.2] ± [0.7, 0.2, 0.9]
Tangential moment† (nAm):	23.22	24.62 ± 1.05
Radial moment‡ (nAm):	14.86	15.38 ± 0.73

	True Values	Fitted Values (mean ± SD)
Case 5b (2-dipole, BEM), Dipole #2		
Location† [x, y, z] (mm):	[−58.0, 28.9, 54.0]	[−57.2, 28.6, 54.1] ± [0.6, 0.2, 0.1]
Tangential moment† (nAm):	19.60	21.00 ± 0.93
Radial moment‡ (nAm):	17.05	17.89 ± 0.38

The tangential moments are the Euclidian sums of the dipole moments alone the two tangential axes., For spherical head models (i.e., Cases 1, 2, and 3), the dipole location and tangential component were obtained exactly with MEG since it does not depend on the conductivity profile (SD = 0). For realistically-shaped BEM head models (i.e., Cases 4 and 5) the dipole location and tangential MEG are insensitive to the conductivity profile. The symbol "†" indicates the analyses for dipole location and tangential dipole moments were conducted for all combinations of the conductivities. The reconstructed radial dipole moments were obtained using the integrated MEG and EEG analysis as described in the main text, and ‡ means that radial dipole moments were estimated along the optimal conductivity profiles (i.e., solid black lines in Figs 3 and 4).

Table 2

Mean values and uncertainties of the fitted dipole location and tangential dipole moments obtained from MEG, and the radial dipole moments from MEG-EEG integration, for a cortical dipole (a) and a subcortical dipole (b), under typical- and high-noise conditions.

(a) Cortical Dipole	**True values**	**Fitted values, typical noise level:**	**Fitted values, high noise level:**
Location [x, y, z] (mm):	[−45.0, 7.2, 47.7]	[−45.0, 7.1, 47.7] ± [0.5, 0.7, 0.6]	[−45.0, 7.3, 47.7] ± [1.0, 1.3, 1.1]
Tangential moment (nAm):	23.18	23.17 ± 0.99	23.23 ± 1.93
Radial moment (nAm):	14.92	14.60 ± 1.36	14.81 ± 2.90
(b) Deep Subcortical Dipole	True values	Fitted values, typical noise level:	Fitted values, high noise level:
Location [x, y, z] (mm):	[−22.5, 3.6, 23.8]	[−22.4, 3.7, 23.7] ± [2.1, 2.8, 2.3]	[−22.8, 4.1, 24.0] ± [3.7, 4.9, 4.1]
Tangential moment (nAm):	23.18	23.56 ± 4.08	23.67 ± 8.08
Radial moment (nAm):	14.92	15.12 ± 4.57	14.90 ± 7.88

Table 3

Locations, tangential, and radial dipole moments obtained from the integrated MEG and EEG analysis of simultaneously recorded MEG and EEG M20/N20 component evoked by median nerve stimuli. The SD shows the variation of the source parameters when we vary $\sigma_{scalp}(=\sigma_{brain})$ and σ_{skull} independently.

(a) Conductivity-related variations	**Left SI evoked by right median-nerve stimuli**	**Right SI evoked by left median- nerve stimuli**
Location[†] [x, y, z] (mm)	[48.5, 19.1, 97.5] ± [0.3, 0.3, 0.5]	[−48.0, 16.8, 95.7] ± [0.4, 0.5, 0.8]
Tangential Moment[†] (nAm)	38.6 ± 0.4	34.1 ± 0.4
Radial Moment[‡] (nAm)	13.6 ± 0.8	−7.0 ± 0.4
(b) Impacts from sensor- and brain-noises: Bootstrapping	Left SI evoked by right median-nerve stimuli	Right SI evoked by left median- nerve stimuli
Location [x, y, z] (mm)	[48.5, 19.0, 97.3] ± [0.6, 0.6, 0.7]	[−48.3, 17.0, 95.4] ± [0.6, 0.7, 0.8]
Tangential Moment (nAm)	38.8 ± 0.7	33.9 ± 0.8
Radial Moment (nAm)	13.4 ± 0.8	−7.2 ± 0.9